A New Class of Changing-Look LINERs

Sara Frederick,[1] Suvi Gezari,[1, 2] Matthew J. Graham,[3] S. Bradley Cenko,[2, 4] Sjoert van Velzen,[5, 6] Daniel Stern,[7]
Nadejda Blagorodnova,[3] Shrinivas R. Kulkarni,[3] Lin Yan,[8] Kishalay De,[3] U. Christoffer Fremling,[3] Tiara Hung,[9]
Erin Kara,[1, 2, 10] David L. Shupe,[11] Charlotte Ward,[1] Eric C. Bellm,[12] Richard Dekany,[8] Dmitry A. Duev,[3]
Ulrich Feindt,[13] Matteo Giomi,[14] Thomas Kupfer,[15] Russ R. Laher,[11] Frank J. Masci,[11] Adam A. Miller,[16, 17]
Chow-Choong Ngeow,[18] Maria T. Patterson,[12] Michael Porter,[8] Ben Rusholme,[11] Jesper Sollerman,[19] and
Richard Walters[8]

[1]*Department of Astronomy, University of Maryland, College Park, MD 20742, USA*

[2]*Joint Space-Science Institute, University of Maryland, College Park, MD 20742, USA*

[3]*Division of Physics, Mathematics, and Astronomy, California Institute of Technology, Pasadena, CA 91125, USA*

[4]*Astrophysics Science Division, NASA Goddard Space Flight Center, MC 661, Greenbelt, MD 20771, USA*

[5]*Department of Astronomy, University of Maryland, College Park, MD 20742*

[6]*Center for Cosmology and Particle Physics, New York University, NY 10003*

[7]*Jet Propulsion Laboratory, California Institute of Technology, 4800 Oak Grove Drive, Mail Stop 169-221, Pasadena, CA 91109, USA*

[8]*Caltech Optical Observatories, California Institute of Technology, Pasadena, CA 91125, USA*

[9]*Department of Astronomy and Astrophysics, University of California, Santa Cruz, CA 95064, USA*

[10]*X-ray Astrophysics Laboratory, NASA/Goddard Space Flight Center, Greenbelt, Maryland 20771, USA*

[11]*IPAC, California Institute of Technology, 1200 E. California Blvd, Pasadena, CA 91125, USA*

[12]*DIRAC Institute, Department of Astronomy, University of Washington, 3910 15th Avenue NE, Seattle, WA 98195, USA*

[13]*The Oskar Klein Centre, Physics Department, Stockholm University, Albanova University Center, SE 106 91 Stockholm, Sweden*

[14]*Institute of Physics, Humboldt Universitæt zu Berlin, Newtonstraße 15, 12489 Berlin, Germany*

[15]*Kavli Institute for Theoretical Physics, University of California, Santa Barbara, CA 93106, USA*

[16]*Center for Interdisciplinary Exploration and Research in Astrophysics (CIERA) and Department of Physics and Astronomy, Northwestern University, 2145 Sheridan Road, Evanston, IL 60208, USA*

[17]*The Adler Planetarium, Chicago, IL 60605, USA*

[18]*Graduate Institution of Astronomy, National Central University, Taoyuan 32001, Taiwan*

[19]*The Oskar Klein Centre & Department of Astronomy, Stockholm University, AlbaNova, SE-106 91 Stockholm, Sweden*

ABSTRACT

We report the discovery of six active galactic nuclei (AGN) caught "turning on" during the first nine months of the Zwicky Transient Facility (ZTF) survey. The host galaxies were classified as LINERs by weak narrow forbidden line emission in their archival SDSS spectra, and detected by ZTF as nuclear transients. In five of the cases, we found via follow-up spectroscopy that they had transformed into broad-line AGN, reminiscent of the changing-look LINER iPTF16bco. In one case, ZTF18aajupnt/AT2018dyk, follow-up *HST* UV and ground-based optical spectra revealed the transformation into a narrow-line Seyfert 1 (NLS1) with strong [Fe VII, X, XIV] and He II λ4686 coronal lines. *Swift* monitoring observations of this source reveal bright UV emission that tracks the optical flare, accompanied by a luminous soft X-ray flare that peaks $\sim$60 days later. *Spitzer* follow-up observations also detect a luminous mid-infrared flare implying a large covering fraction of dust. Archival light curves of the remainder of the sample from CRTS, ATLAS, and ASAS-SN reveal similar flare-like deviations from a quiescence, and constrain the onset of the optical nuclear flaring. Here we present the systematic selection and follow-up of this new class of changing-look LINERs, compare their properties to previously reported changing-look Seyfert galaxies, and conclude that they are a unique class of transients related to physical processes associated with the LINER accretion state.

Keywords: accretion, accretion disks — galaxies: active — galaxies: nuclei — quasars: emission lines — relativistic processes — surveys

Corresponding author: Sara Frederick
sfrederick@astro.umd.edu

1. INTRODUCTION

The observed diversity in the optical spectra of AGN, with well-defined systematic trends known as the eigenvector relations, are understood to be a function of both orientation

as well as accretion rate (e.g. Shen & Ho 2014). "Changing-look" active galactic nuclei (CLAGN) are a growing class of objects that are a challenge to this simple picture, in that they demonstrate the appearance (or disappearance) of broad emission lines and a non-stellar continuum, changing their classification between type 1.8-2 (narrow-line) to type 1 (broad-line) AGN (or vice versa) on a timescale of years. The nature of this spectral transformation is most often attributed to changes in accretion rate (Shappee et al. 2014; Runnoe et al. 2016; MacLeod et al. 2016; Oknyansky et al. 2016; Ruan et al. 2016; Sheng et al. 2017), but the mechanism(s) driving these sudden changes is still not well understood (e.g. Lawrence 2018; Stern et al. 2018).

One of the known changing look quasars (CLQs), iPTF16bco (Gezari et al. 2017), was caught "turning-on" in the iPTF survey into a broad-line quasar from a low-ionization nuclear emission-line region galaxy (LINER). LINERs are distinguished from Seyfert 2 (Sy 2) spectra via the relatively strong presence of low-ionization or neutral line emission from [O I] $\lambda6300$, [O II] $\lambda3727$, [N II] $\lambda\lambda6548$, 6583, and [S II] $\lambda\lambda6717$, 6731; a lower [O III] $\lambda5007$/Hβ flux ratio; and a lower nuclear luminosity. However, the status of LINERs as low-luminosity AGN remnants is a topic of debate, as weak emission in some LINERs could also be powered by shocks, winds, outflows, or photoionization from post-AGB stellar populations (Ho et al. 1993; Filippenko 1996; Bremer et al. 2013; Singh et al. 2013). LINER galaxies are the largest AGN sub population, and may constitute one-third of all nearby galaxies (Heckman 1980; Ho et al. 1997b), yet iPTF16bco was one of only three cases of a CLAGN in a LINER out of the nearly 70 known CLAGN at the time.[1] Furthermore, as a LINER, iPTF16bco had a lower inferred accretion rate in its low state ($L/L_{\rm Edd} \lesssim 0.005$, Gezari et al. 2017) compared to the majority of previously discovered CLAGN (MacLeod et al. 2019), implying a much more dramatic transformation.

We report the discovery of six new CLAGN, all classified as LINER galaxies by their archival SDSS spectra, detected as nuclear transients by the Zwicky Transient Facility (ZTF; Graham et al. (2019); Bellm et al. (2019a)), and spectroscopically confirmed as "changing-look" to a NLS1 or broad-line (type 1) AGN spectral class. One of these nuclear transients, ZTF18aajupnt/AT2018dyk, was initially classified as a candidate tidal disruption event (TDE) from the presence of Balmer and He II emission lines (Arcavi et al. 2018). Here, we show that the ZTF light curve, together with our sequence of follow-up optical spectra and UV and X-ray monitoring with *Swift* and follow-up UV spectra with *HST*, are more consistent with a CLAGN classification. It was previously thought that, although they

are commonly found in Seyferts, coronal emission lines (such as [Fe VII] $\lambda6088$) should never be exhibited by LINER-like galaxies by definition (e.g. Corbett et al. 1996). However, here we also report the surprising appearance of coronal lines coincident with an increase in UV/optical and soft X-ray continuum emission and broad Balmer emission consistent with a NLS1 in this galaxy previously classified as a LINER.

This paper is organized as follows. In Section 2, we present our sample selection of nuclear transients in LINERs, information on the host galaxies, ZTF and archival optical light curves, optical spectroscopic observations, and multiwavelength follow-up observations of ZTF18aajupnt/AT2018dyk, including details of the data reduction involved. In Section 3, we introduce a new class of changing-look LINERs, and compare their properties to previously reported Seyfert CLAGN, focusing on the particularly interesting case of ZTF18aajupnt/AT2018dyk, which transformed from a LINER to a NLS1. In Section 4 we discuss the results of our analysis, the conclusions of which are summarized in Section 5.

Throughout the paper we use UT dates, and assume the following cosmology for luminosity calculations: $H_0 = 70$ km s^{-1} Mpc^{-1}, $\Omega_\Lambda = 0.73$ and $\Omega_M = 0.27$. We have corrected for Galactic extinction toward the sources ($E(B - V) = 0.0164$ mag) where explicitly stated. All magnitudes are in the AB system, and all uncertainties are at the 1σ level unless otherwise noted. We adopt the definition for a quasar from the SDSS DR7 quasar catalog (Schneider et al. 2010), as having an apparent i-band PSF magnitude fainter than 15 and an absolute i-band magnitude brighter than -22.

2. DISCOVERY AND OBSERVATIONS

2.1. *Sample Selection Criteria*

We selected CLAGN candidates first flagged as nuclear transients in the ZTF alert stream (described further in Section 2.2) and with a cross-match within $1''.0$ of a LINER or type 2 Seyfert galaxy in the Portsmouth Catalog's narrow-line ratio BPT classifications[2] (Bolzonella et al. 2000; Thomas et al. 2013). Those classifications, described further in Section 3.1, are based on stellar population and emission line fits to SDSS DR12 spectra, performed with Penalized Pixel Fitting (pPXF; Cappellari & Emsellem (2004); Cappellari (2016)) and Gas and Absorption Line Fitting (GANDALF; Sarzi et al. (2017)), respectively. In this study, we focus on the "LINER CLAGN" that emerged as a new class of changing look AGN and display the most dramatic spectral variability of the CLAGN in our ZTF sample (we reserve discussion of the complementary sample of Seyfert CLAGN for a forthcoming publication).

2.2. *ZTF Light Curve*

---

[1] We note that the other two known so-called CL LINERs, NGC 1097 (Storchi-Bergmann et al. 1993) and NGC 3065 (Eracleous & Halpern 2001) are, or are reminiscent of, transient double peaked emitters, which may be distinct from changing look AGN.

[2] https://www.sdss.org/dr12/spectro/galaxy_portsmouth/#kinematics

ZTF surveys the extragalactic[3] Northern Sky in two modes: a public Mid-Scale Innovations Program (MSIP) survey of 15,000 deg^2 of sky every 3 nights in g and r filters, and a high-cadence ZTF partnership survey of 3400 deg^2 with a dense cadence of 6 epochs each in g and r filters per night. It also surveys in i-band every 4 nights with a footprint of 10725 deg^2 (Bellm et al. 2019b). PTF and iPTF (2009–2016; Law et al. (2009); Rau et al. (2009)) also utilized Palomar Observatory's Samuel Oschin 48" Schmidt telescope; the camera upgrade for ZTF has a 47 deg^2 FoV and reaches 20.5 r-band mag in 30 seconds exposures, with a more efficient areal survey speed of 3760 deg^2 hr^{-1}. Images are processed each night by the Infrared Processing and Analysis Center (IPAC) pipeline (Masci et al. 2019), where difference imaging and source detection are performed to produce a transient alert stream (Patterson et al. 2019), distributed to the GROWTH Marshal (Kasliwal et al. 2019) and other brokers via the University of Washington Kafka system. van Velzen et al. (2019) presented details of the nuclear transients filtering procedure.

All transients in the sample were discovered in 2018 between April and November, all in the ZTF MSIP survey (specific dates are summarized in Table 1). ZTF18aajupnt[4] was also detected in the ZTF Partnership survey on 2018 May 31, and (as it was detected in both surveys in the same night) was registered publicly to the Transient Name Server (TNS) as AT2018dyk. Transients were required to have a real-bogus (RB) score ≥ 0.5 as classified by ZTF machine learning (Mahabal et al. 2019). Further details on the transients, including discovery difference absolute magnitudes, are in Table 1.

The optical photometry for ZTF18aajupnt/AT2018dyk, ZTF18aasuray, ZTF18aahiqfi, ZTF18aaidlyq, ZTF18aasszwr, and ZTF18aaabltn is comprised of 398, 200, 35, 35, 143, and 207 images, respectively, shown in Figure 1. We consider only observations with difference image detections classified as real (with RB score≥ 0.5 on a scale where 0 is bogus and 1 is real). The ZTF optical difference imaging light curves show only the transient nuclear emission in the g- and r-bands. The transients are localized to within $0.''19^{+0.''28}_{-0.''19}$ (ZTF18aajupnt/AT2018dyk), $0.''09\pm0.''26$ (ZTF18aasuray), $0.''11^{+0.''33}_{-0.''11}$ (ZTF18aahiqfi), $0.''06^{+0.''33}_{-0.''06}$ (ZTF18aaidlyq), $0.''10^{+0.''20}_{-0.''10}$ (ZTF18aasszwr), and $0.''15\pm0.''15$ (ZTF18aaabltn) of their host galaxy nuclei, well within our nuclear selection criterion of $< 0.''5$.

To quantify the amplitude of the flux increase relative to the host galaxy flux, and to compare to variability of

CLAGN measured from imaging surveys that do not perform image subtraction, as in Hung et al. (2018), we add the flux of the host galaxy to the transient flux, to get a variability amplitude, $\Delta m_{\rm var} = m_{r,\rm tot} - m_{r,\rm host}$, where $m_{r,\rm tot} = -2.5\log(10^{-m_r/2.5+-m_{r,\rm host}/2.5})$, and m_r represents the brightest transient ZTF r-band magnitude and $m_{r,\rm host}$ is the archival host magnitude from SDSS DR14. We find $\Delta m_{\rm var}$ values ranging from -0.12 to -0.81 mag for the sources in our sample, with 3 out of 5 below the CLAGN candidate selection criteria of an amplitude of $\Delta r > 0.5$ mag between SDSS and Pan-STARRS1 imaging observations adopted by MacLeod et al. (2019).

ZTF18aajupnt (AT2018dyk; discussed more in Section 2.5), ZTF18aasuray, and ZTF18aasszwr display a slow months-long rise and plateau (although a visibility gap makes this unclear for ZTF18aasuray) with a constant color, and gradual decline, with ZTF18aasszwr exhibiting a second rise and ZTF18aajupnt/AT2018dyk growing redder in the latest observations. All other transients in the sample show flaring in the light curves (see Figure 1) but with less distinct trends, characteristic of broad-line AGN variability viewed in difference imaging (Choi et al. 2014).

2.3. *Capturing the Transition in Archival Light Curves*

Although difference imaging is a useful real-time discovery mechanism for these nuclear transients, archival optical photometric observations can fill in the details of the timing of the transition to its "on" state. With archival light curves extending over a baseline of 13 years from the Catalina Real-time Transient Survey (CRTS; Drake et al. 2009), the All-Sky Automated Survey for Supernovae (ASAS-SN; Shappee et al. 2014[5]), and Asteroid Terrestrial-impact Last Alert System (ATLAS; Tonry et al. 2018), and ZTF aperture photometry from the IPAC pipeline measured from the static images, we uncover an intriguing uniformity in the events (Figure 2). Each source in the sample went from lacking any significant variability to flaring dramatically and, for those observed long enough, subsequently declining (ZTF18aaabltn continues to rise smoothly). As not all sources in the sample have peaked, we define the transition timescale for each source reported in Table 1 as being from the onset of each flare to the spectroscopic confirmation of the appearance of a blue continuum and broad line emission (except iPTF16bco, for which the onset time was constrained by archival and follow up X-ray observations; Gezari et al. (2017)). Turn-on timescales, absolute r-band magnitudes at the time of detection with ZTF, variability amplitude relative to the host galaxy flux, and new AGN class following the change are summarized in Table 1 for all transients in the sample. We discuss the details of each source's flaring individually below.

ZTF18aajupnt/AT2018dyk — ZTF-matched aperture photometry in g band shows that

---

[3]Additional public and private allocations are made to survey the Galactic Plane at higher cadence. See Bellm et al. (2019b) for details.

[4] As ZTF given names are typically a mouthful of letters (appropriately so, due to the requirement of naming upwards of a million alerts per night), the ZTF Black Holes Working Group has informally begun naming TDEs from a fictional world with no shortage of characters: HBO's *Game of Thrones*. As it was initially thought to be a TDE, ZTF18aajupnt/AT2018dyk was affectionately dubbed "Tyrion Lannister".

[5]http://www.astronomy.ohio-state.edu/~assassin

Table 1. Basic data for the changing look LINER sample. We list redshifts from the Portsmouth SDSS DR12 catalog (Thomas et al. 2013), which is described in Section 2.1. Transition timescales δt are roughly constrained based on the time delay between the onset of variability detected in the host in the archival light curves, and the time of the first spectrum taken in the type 1 AGN state. Estimates of star formation rate by Chang et al. (2015) are from SDSS+WISE SED model fitting. Δm is the variability magnitude change defined in Eq. 3 of Hung et al. (2018) as $\Delta m = -2.5\log(10^{-m_{r,host}/2.5} + 10^{-m_r/2.5}) - m_{r,host}$, where m_r represents the brightest, transient r-band magnitude in the difference-imaging light curve. ZTF18aajupnt/AT2018dyk, described further in Section 3.6 is the least luminous transient, and has the nearest host of the sample.

Name	RA (hh:mm:ss.ss)	Dec (dd:mm:ss.ss)	z	D_{Lum} (Mpc)	Discovery Date	$M_{Discovery}$ (mag)	δt (yr)	Host Type[a]	log SFR [$M_\odot$ yr^{-1}]	Δm_{var} (mag)	High State
ZTF18aajupnt[b]	15:33:08.01	+44:32:08.2	0.0367	158	2018 May 31[c]	−16.59	<0.3	Spiral (SBb D)	0.177	−0.18	NLS1
ZTF18aasuray[d]	11:33:55.83	+67:01:08.0	0.0397	171	2018 May 10	−17.80	<6.8	Spiral (SBa(r)[e])	0.147	−0.06	Seyfert 1
ZTF18aahiqfi[f]	12:54:03.80	+49:14:52.9	0.0670	296	2018 April 8	−18.25	<0.6	Elliptical	−0.058	−0.12	quasar
ZTF18aaidlyq[g]	09:15:31.06	+48:14:08.0	0.1005	457	2018 April 11	−19.09	<0.7	Spiral (Sb D)	0.092	−0.29	quasar
ZTF18aaabltn[h]	08:17:26.42	+10:12:10.1	0.0458	199	2018 Sept 15	−17.62	<2.6	Elliptical	0.227	−0.81	quasar
ZTF18aasszwr[i]	12:25:50.31	+51:08:46.5	0.1680	813	2018 Nov 1	−20.40	<5.3	Elliptical	1.267	−0.72	quasar

[a] Kuminski & Shamir (2016)
[b] hosted in SDSS J153308.02+443208.4/IRAS F15313+4442/2MASX J15330803+4432086
[c] In ZTF Partnership Survey
[d] TNS name AT2018cdp; hosted in SDSS J113355.93+670107.0/2MASX J11335602+6701073
[e] Hernández-Toledo et al. (2010) (Kuminski & Shamir (2016) reported nearly a 50% probability for both spiral and elliptical type for this host galaxy.)
[f] hosted in SDSS J125403.78+491452.8/2MASX J12540375+4914533
[g] TNS name AT2018ivp; hosted in SDSS J091531.04+481407.7
[h] TNS name AT2018gkr; hosted in SDSS J081726.41+101210.1/2MASX J08172642+1012101
[i] hosted in SDSS J122550.30+510846.3/2MASX J12255033+5108461

ZTF18aajupnt/AT2018dyk began flaring some time before 2018 March (58200 MJD) ~2 months prior to discovery in difference imaging on 2018 May 31, and 3 months prior to confirmation of a spectroscopic change. The most recent difference imaging photometry shows a slow decline at constant color. Transition timescale: < 0.3 years, the fastest in the sample.

ZTF18aahiqfi — The rise (seen in ZTF g-band matched photometry) starts approximately at 2017 Sept (58000 MJD), 7 months prior to its spectroscopic change. It peaks around 2018 May (58250 MJD; ~1 month after discovery with ZTF difference imaging on 2018 April 8) and subsequently shows a sharp decline. Prior to this flaring, Catalina Real-time Transient Survey (CRTS shown in the left panel of Figure 2; Drake et al. (2009)) observations in V-band and ASAS-SN showed no variability above the 0.1 mag level. Transition timescale: < 0.6 years.

ZTF18aaidlyq — This source displayed a slight flare in ASAS-SN data just after 2017 Sept (58000 MJD), 7 months prior to detection in ZTF difference imaging and 8 months prior to spectroscopic confirmation of the existence of a BLR, but was faint and quiescent in CRTS beginning in 2005 May (note that this source is near a bright star). Transition timescale: < 0.7 years.

ZTF18aasuray — Discovery with ZTF difference imaging occurred on 2018 May 10 and shows a slow symmetric rise and decline lasting 300 days. ZTF18aasuray displayed flaring in ASAS-SN data beginning around 2011 Aug (55800 MJD), 6.8 years prior to spectroscopic confirmation of the changing look which occurred on 2018 June 21. Prior to this flaring, Catalina Real-time Transient Survey (CRTS
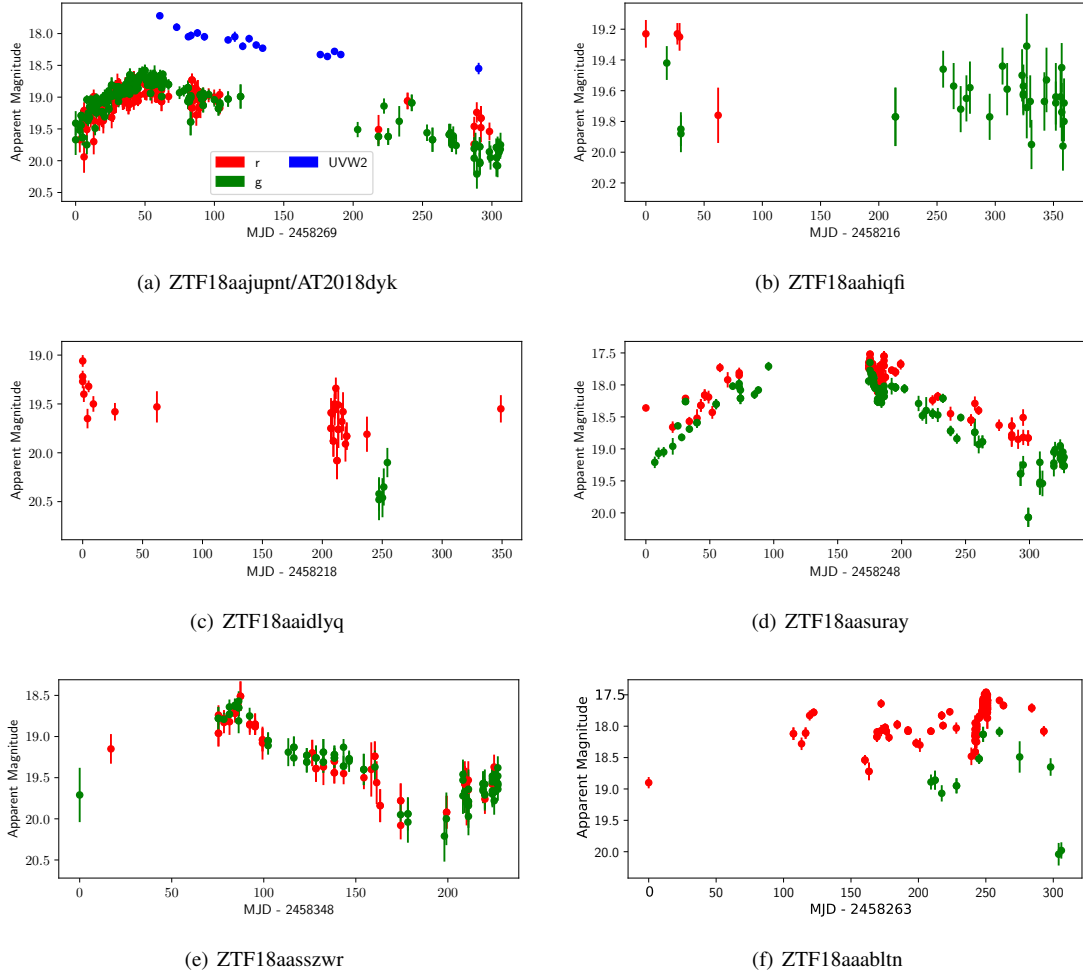
shown in the left panel of Figure 2; Drake et al. (2009)) observations in V-band showed no variability above the 0.1 mag level. Transition timescale: < 6.8 years.

ZTF18aasszwr — The rise is visible in CRTS around 2018 July (56500 MJD), after which it may have plateaued for a time. Most recently there has been a sharp rise and decline around 2018 May (58250 MJD), with the peak reaching > 1 mag above original levels. The transition from quiescence thus happened roughly in real time, and was observed with difference imaging 4 months after the flaring began, with the spectroscopic change confirmed within 5.3 years of the initial rise time, and within 5 months of the onset of the most recent flare. We note that two decades ago, ZTF18aasszwr was a variable (rms = 0.14 mJy) radio source between the NRAO VLA Sky Survey and Faint Images of the Radio Sky at Twenty centimeters (NVSS and FIRST; Ofek & Frail 2011), with a peak flux density at 1.4 GHz of $F_\nu = 2.17$ mJy. Transition timescale: < 5.3 years.

ZTF18aaabltn — CRTS, ATLAS and ASAS-SN show a continuous rise starting around 2016 April (57500 MJD) but this disregards some slight flaring (by 0.2 mag) events at 2008 Nov and just before 2014 Dec (57000 MJD), with both returning to very flat pre-activity levels. This constrains the spectroscopic change to happening within 1000 days (< 2.7 years) of the flare start time, the first large flare occurring within 9 months of being observed to be a LINER in 2007 Feb. Transition timescale: < 2.6 years.

iPTF16bco — CRTS photometry shows a flare beginning around 2012 March (56000 MJD), 8 years after being observed to be a LINER and 4 years prior to discovery and classification of a quasar in iPTF, and the latest ZTF g-band

(a) ZTF18aajupnt/AT2018dyk

(b) ZTF18aahiqfi

(c) ZTF18aaidlyq

(d) ZTF18aasuray

(e) ZTF18aasszwr

(f) ZTF18aaabltn

Figure 1. Light curves of the CL LINER sample. Red points represent *r*-band difference imaging photometry data taken with the Palomar 48-inch (P48), green points *g*-band difference imaging photometry, and the blue points are the UVW2 *Swift* photometry in the light curve of ZTF18aajupnt/AT2018dyk, which tracks the plateau in the optical uncharacteristic of either TDEs or SNe. Note the differences in scale.

data shows it declining rapidly. However, archival XMM Slew Survey observations constrain the onset of the X-ray source detected by Swift in its broad-line state to < 1.1 years before (Gezari et al. 2017). Transition timescale: < 1.1 years.

2.4. *Host Galaxy Morphology*

Images of the six transients' host galaxies from SDSS are shown in Figure 3, and basic data including the hosts' names, matched coordinates, redshifts, luminosity distances, morphological types, and star formation rates (SFRs) are summarized in Table 1. The SFR estimates by Chang et al. (2015) were obtained through Multi-wavelength Analysis of Galaxy Physical Properties (MAGPHYS; da Cunha et al. (2012)) model fitting of dust extinction/emission, and SEDs constructed from WISE+SDSS (WISE: Wright et al. (2010)) matched photometry of present-epoch galaxies (we note that SFRs for only two AGN in our sample were measured by Chang et al. (2015), the rest did not fit their criteria). The bulges of the LINERs' hosts are similar in apparent color

and extent, but the host of ZTF18aaidlyq exhibits evidence for a bar and ring, and the host of ZTF18aaabltn exhibits apparent elongation. The host of ZTF18aajupnt/AT2018dyk stands out in the sample as the only gas-rich spiral galaxy, and we note that NLS1s typically occur in spiral-type galaxies (Crenshaw et al. 2003). Black hole masses estimated from the host galaxy luminosity, bulge mass, and velocity dispersions derived from the SDSS host imaging and spectra have been measured in Section 3.2 and are summarized in Table 2.

2.5. *Optical Spectroscopy*

We obtained spectral follow-up of nuclear transients in known LINERS and Sy 2 galaxies as described in Section 2.1 to confirm changing-look AGN candidates, as neither "true" narrow-line Sy 2s nor LINERs are expected to vary significantly. We observed ZTF18aahiqfi, ZTF18aaidlyq, and ZTF18aasuray with the Deveny spectrograph on the Discovery Channel Telescope (DCT; spectral coverage of 3600-8000 Å) with a 1″5 wide slit,
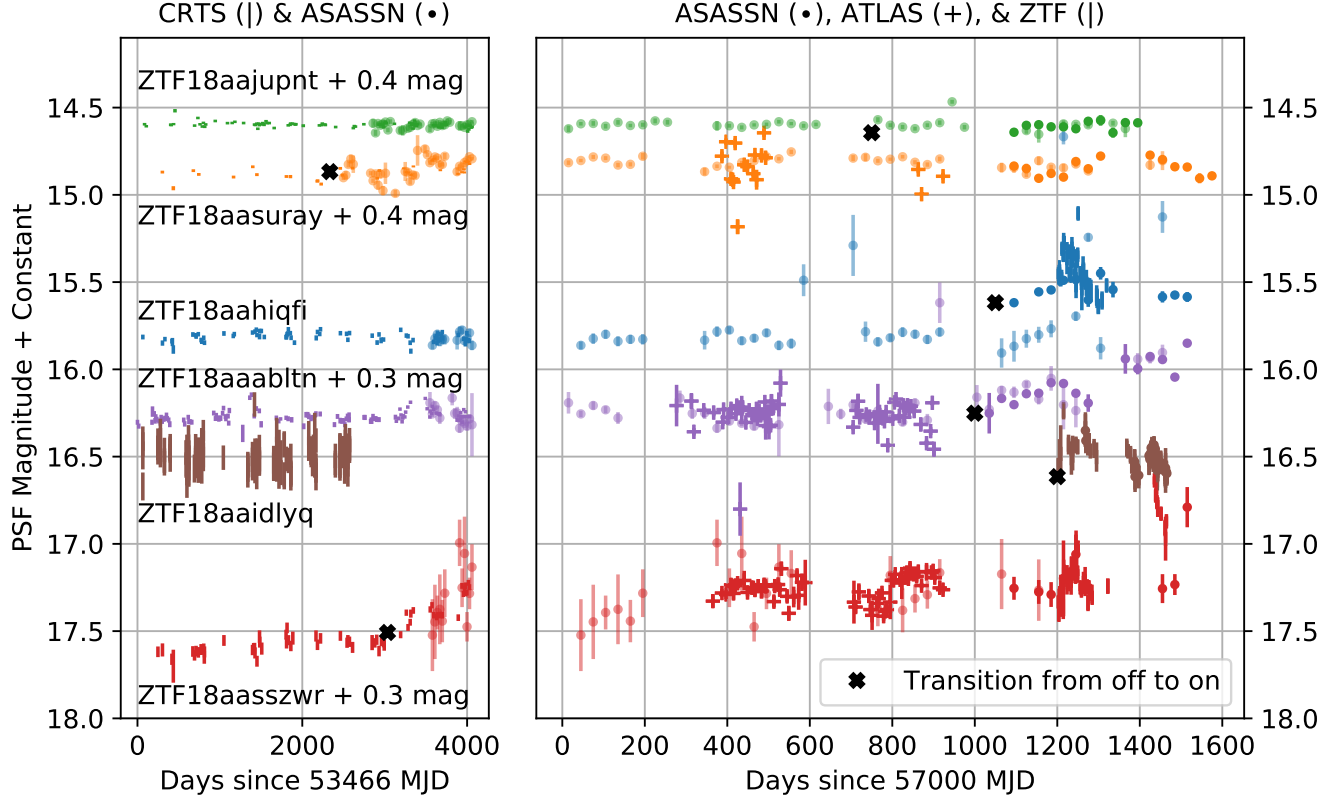
Figure 2. Archival light curves of the CL LINER sample summarized in Section 2.3. The left panel shows years to decades of quiescence (in the "off" state while these were still LINER galaxies) observed by CRTS, followed by slow flares in the faintest sources ZTF18aasszwr, ZTF18aaabltn, and ZTF18aahiqfi. The right panel shows the rise, flaring, and decline of the sources caught by ZTF+ATLAS+ASASSN g-band observations at these various stages. The estimated transition time listed in Section 2.3 for each object is marked by a black "x". When two filters are shown for the same instrument, the redder is shown as more transparent, as in the case of the ASAS-SN g and V photometric points shown.

Table 2. Properties of the host galaxies of our sample of changing-look LINERs from ZTF and iPTF. We also show M_{BH} calculated in Section 3.2 from the host galaxy luminosity, mass, and velocity dispersion, respectively.

Name	$M_{r,host}$[a]	$\log M_{Bulge}$[b]	$\sigma_\star$[c]	λL_{5100A}	$FWHM_{H_\beta}$	$\log M_{BH,M_r}$[d]	$\log M_{BH,Bulge}$[e]	$\log M_{BH,\sigma\star}$[f]	$\log M_{BH,vir}$	L/L_{Edd}[g]
	(mag)	$[M_\odot]$	(km s^{-1})	(10^{43} erg s^{-1})	(km s^{-1})	$[M_\odot]$	$[M_\odot]$	$[M_\odot]$	$[M_\odot]$	
ZTF18aajupnt	−22.00	10.66±0.15	150	0.49±0.11	939±28	8.0	7.8	7.6	6.4	0.09
ZTF18aasuray	−21.70	10.73±0.15	230	10.6±0.4	4270±218	7.9	7.9	8.4	8.0	0.03
ZTF18aaidlyq	−21.64	-	120	12.7±2.3	7726±458	7.9	-	8.2	8.5	0.06
ZTF18aahiqfi	−21.63	-	210	4.1±0.5	8809±723	7.9	-	7.2	8.3	0.2
ZTF18aasszwr	−22.19	11.19±0.15	180	57.0±1.9	6461±846	8.1	8.3	7.9	8.8	0.5
ZTF18aaabltn	−20.62	-	140	0.8±0.2	5195±648	7.3	-	7.5	8.0	0.2
iPTF16bco	−22.21	-	176	17.3±11.0	4183±213	8.4	-	7.9	8.1	0.05

[a]Computed from the r-band de Vaucouleurs / exponential disk profile model fit magnitude from the SDSS DR14 photometric catalog.
[b]Computed from broadband SED fits to photometric measurements of SDSS DR 7 galaxies (Mendel et al. 2014).
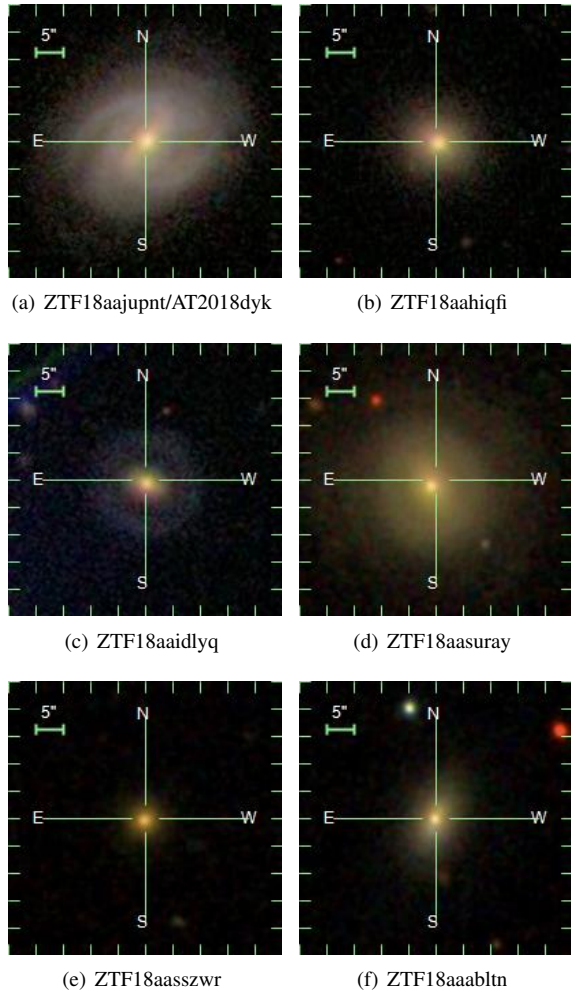[c]Measured from the SDSS spectrum using the PPXF method.
[d]McLure & Dunlop (2002)
[e]Häring & Rix (2004)
[f]Tremaine et al. (2002)
[g]In high state; $M_{BH,\sigma\star}$ was employed to obtain the black hole masses used in computing the Eddington ratio (see Section 3.5).

central wavelength of 5800 Å and exposure times of 2×900, 2×1200, and 1400 seconds on 2018 April 11, May

(a) ZTF18aajupnt/AT2018dyk

(b) ZTF18aahiqfi

(c) ZTF18aaidlyq

(d) ZTF18aasuray

(e) ZTF18aasszwr

(f) ZTF18aaabltn

Figure 3. Composite *ugriz* color SDSS images of the host galaxies of the changing look LINER sample. Their individual morphological classifications are listed in Table 1.

06, and June 21, respectively. The DCT spectra were reduced with standard IRAF routines, corrected for bias and flat-fielding, and combined into a single 2D science frame. Wavelength and flux calibration were done via a comparison with spectra of an arc lamp and the flux standard Feige 34, respectively. The spectra have not been corrected for telluric absorption. We found that the Balmer lines of ZTF18aahiqfi, ZTF18aaidlyq, and ZTF18aasuray had gotten dramatically stronger and broader compared to archival SDSS spectra of their hosts, obtained more than a decade prior (in April 2003, Dec 2002, and Feb 2001, respectively).

ZTF18aasszwr and ZTF18aaabltn showed similar striking spectral changes when they were followed up on 2018 Dec 3 and 9 using the Spectral Energy Distribution Machine (SEDM; Blagorodnova et al. 2018b) IFU spectrograph on the Palomar 60-inch (P60; Cenko et al. 2006) operating as part of ZTF. Both displayed broader emission lines and bluer continuua compared to archival LINER spectra (from

Table 3. Spectroscopic Legacy and Follow-up Observations of ZTF18aajupnt/AT2018dyk.

Obs UT	Instrument	Exposure (s)	Reference
2002 July 11	SDSS	28816	Abolfathi et al. (2018)
2018 June 12	Palomar 200" DBSP	2400	This work
2018 July 22	Palomar 60" SED Machine	2430	This work
2018 July 30	*Swift* XRT	40400	This work
2018 Aug 7	Keck LRIS	300	This work
2018 Aug 11	*XMM* EPIC pn	11906	This work
2018 Aug 12	Palomar 60" SED Machine	2430	This work
2018 Aug 12	FTN FLOYDS-N	3600	Arcavi et al. (2018)
2018 Aug 21	Gemini GMOS-N	600	This work
2018 Sept 1	*HST* STIS	2859	This work
2018 Sept 12	DCT Deveny	2400	This work

Feb 2007 and Jun 2004, respectively). The SEDM data were reduced with pySEDM (Rigault et al. 2019).

See the spectral comparisons for all CLAGN in the sample in Figure 4, and zoom-ins of the emission lines in the "off" states in Figures 18, 19, and "on" states in Figure 20 of the Appendix. The hosts of all six transients in this sample were originally classified as LINERs in SDSS, however we re-measured the diagnostic narrow-line ratios in Section 3.1, and find that the majority of the sample is on the borderline between a LINER and Seyfert classification.

Due to its similarity to a TDE at early times, we promptly initiated a multi-wavelength follow-up campaign of ZTF18aajupnt/AT2018dyk which we describe in the following sections. Following the discovery of a blue continuum with the Double Spectrograph (DBSP) of the Palomar 200-inch Hale telescope on 2018 June 12 (PI: David Cook), we monitored ZTF18aajupnt/AT2018dyk with five additional epochs of optical spectroscopy with SEDM on Palomar's 60-inch on 2018 July 22 and Aug 12, LRIS on the Keck I telescope on 2018 Aug 7 (PI: Kulkarni), Gemini GMOS-N on 2018 Aug 21 (PI: Hung), and with Deveny on the DCT on 2018 Sept 12 (PI: Gezari). We detail the configurations of the spectroscopic follow-up observations of ZTF18aajupnt/AT2018dyk in Table 3. During this time, its optical light curve plateaued in a manner strikingly similar to iPTF16bco (shown in Figure 5). It also surprisingly displayed coronal emission lines (those detected are shown in Figures 7 and 21) in a heretofore low-ionization nuclear source.

Figure 6 shows a complete series of spectra obtained for ZTF18aajupnt/AT2018dyk, as well as comparisons to some examples of other AGN and transient types, including the class of extreme coronal line emitters (ECLEs) and the luminous SN IIn SN 2005ip which demonstrated strong coronal line emission (Smith et al. 2009). These spectra were reduced with standard pipelines and procedures for each instrument. Measurements of the flux, luminosity,

(a) iPTF16bco

(b) ZTF18aahiqfi

(c) ZTF18aaidlyq

(d) ZTF18aasuray

(e) ZTF18aasszwr

(f) ZTF18aaabltn
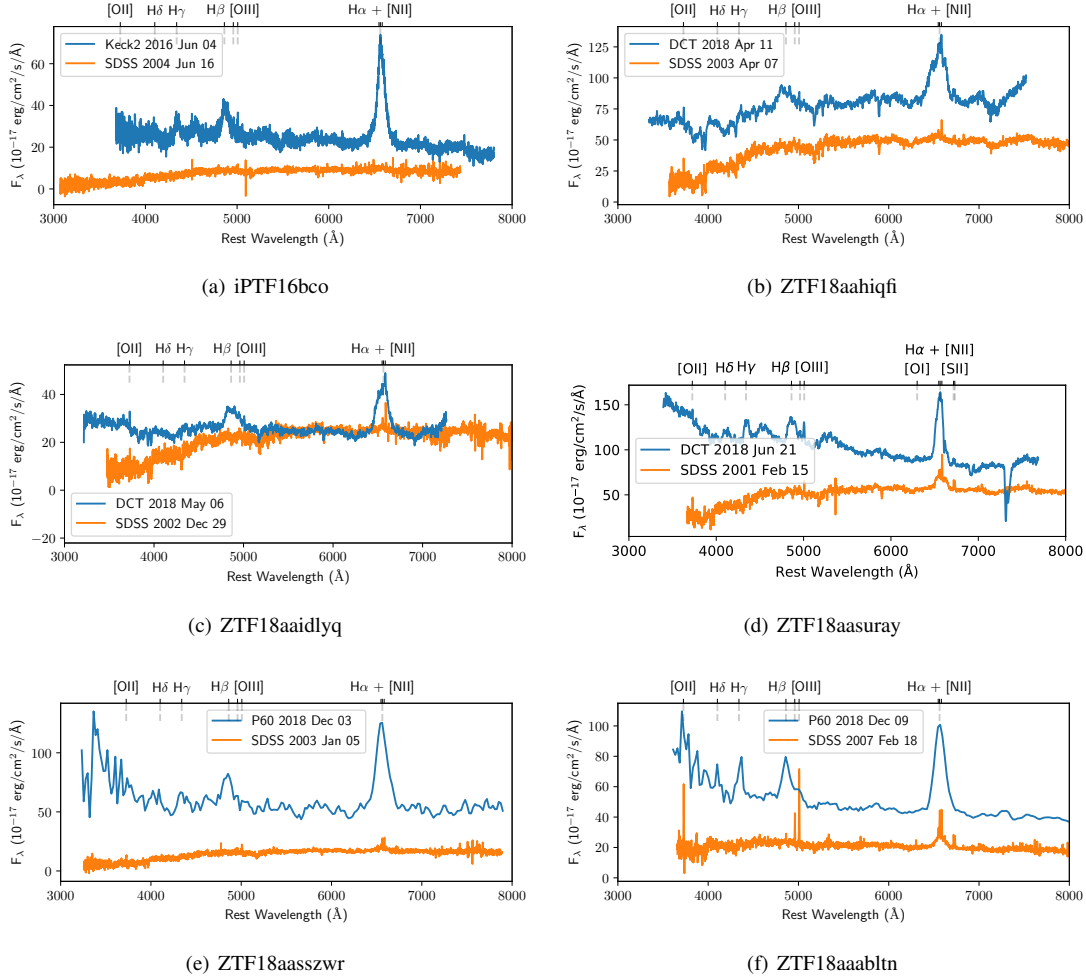
Figure 4. Comparison of early and follow-up spectra of the other CLAGN in the sample. Note that the Palomar 60-inch "P60" spectra have a difference in aperture affecting the flux measurement by a factor of order unity. Detailed follow-up of ZTF18aajupnt/AT2018dyk (not shown here) is presented in Figure 6.

radial velocity, full-width-at-half-maximum (FWHM), and equivalent width of the emission lines, including the coronal emission lines ([Fe XIV] $\lambda 5304$, [Fe VII] $\lambda\lambda 5721, 6088$, [Fe X] $\lambda 6376$ in the spectrum with the highest signal-to-noise detection of the coronal lines is given in Table 4. The FLOYDS-N spectrum from 2018 Aug 12 was reported by Arcavi et al. (2018) to have broad Hα, and both broad and narrow Hβ and He II. At that time, a blue continuum was not obvious in their spectrum. However, we show a power-law blue excess is clearly detected in the residuals of the spectra after subtracting a model for the host galaxy light (Figure 7).

We have corrected for Galactic extinction in the spectra in Figure 6, with color excess $E(B-V) = 0.0164$ mag (from the Schlafly & Finkbeiner (2011) dust map[6]). We use the optical

[6] https://irsa.ipac.caltech.edu/applications/DUST/

correction curve for $R_V = 3.1$ given by Eqs. 3.a. and b. in Cardelli et al. (1989), such that $f_{\rm corr} = f_{\rm obs} 10^{A_\lambda/2.5}$.

2.6. *UV Imaging and Spectroscopy*

We obtained 17 epochs of follow-up imaging of ZTF18aajupnt/AT2018dyk with the Neil Gehrels *Swift* Observatory's (Gehrels et al. 2004) Ultraviolet/Optical Telescope (UVOT; Roming et al. (2005); Poole et al. (2008)) from 2018 July 30 to 2019 Mar 17 with 2−3 ks per epoch in the UVW2 filter ($\lambda_{\rm eff} = 2030$ Å; See Figure 1 and 8). We detected NUV brightening in the nucleus relative to its archival *Galaxy Evolution Explorer* (*GALEX*; Martin et al. (2005)) All-Sky Imaging Survey (AIS) magnitude of $NUV = 19.0$ mag (measured with a 6 arcsec radius aperture).

The source was initially detected with a *Swift* UVW2 = 17.7 mag (measured within a 5 arcsec radius aperture), which then faded to UVW2 = 18.0 mag 20 days later, and then remained roughly at this UV flux over the next 50 days.
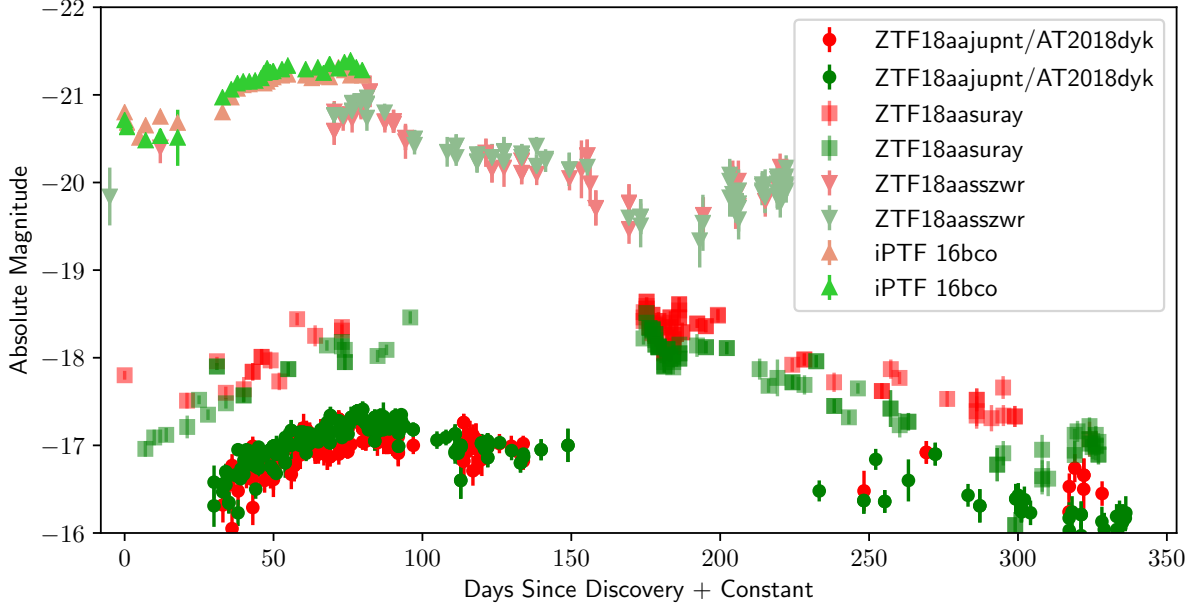
Figure 5. Difference imaging light curves of the CL LINERs with the best-sampled P48 observations in the ZTF sample (ZTF18aajupnt/AT2018dyk, ZTF18aasszwr, and ZTF18aasuray) plotted in absolute magnitude compared to that of CL LINER iPTF16bco (triangle shaped points). ZTF18aasszwr and iPTF16bco are similar in luminosity and more luminous than ZTF18aajupnt/AT2018dyk and ZTF18aasuray by about 2.5 mag. ZTF18aasuray has a much slower evolution and is constantly redder in color, whereas ZTF18aajupnt/AT2018dyk reddens ~280 days into its evolution. The rise of ZTF18aajupnt/AT2018dyk mirrors that of iPTF16bco, whereas the decline appears slower than but similar in shape to that of ZTF18aasszwr.

Table 4. Line measurements for ZTF18aajupnt/AT2018dyk from fits in Figure 21 and used in Figures 16, 13 and 17. The blueshift measured significantly only in Fe X translates to ≈0.0005 c.

	λ (Å)	F_λ (10^{-15} ergs s^{-1} cm^{-2} Å^{-1})	L (10^{39} ergs s^{-1})	v_r (km s^{-1})	FWHM (km s^{-1})	EW (Å)
Hα	6562.80	27.67±0.59	82.4±1.2	57±4	1061±19	56.9±1.5
[NII]λ6548	6548.05	0.21±0.19	0.64±0.37	−612±19	212±59	0.4±0.0
[NII]λ6583	6583.45	1.11±0.15	3.31±0.29	954±10	335±28	7.9±0.2
Hβ	4861.30	9.02±0.32	26.85±0.94	76±8	939±28	18.0±0.7
[OIII]	5006.84	0.96±0.16	2.86±0.47	73±24	489±59	2.1±0.3
HeII	4686.00	3.48±0.29	10.37±0.85	10±28	1157±69	6.7±0.6
[FeXIV]	5304.00	0.45±0.14	1.33±0.40	37±44	546±115	1.0±0.3
[FeVII]λ5721	5721.00	0.81±0.14	2.40±0.41	62±40	795±98	1.6±0.3
[FeVII]λ6088	6088.00	1.08±0.13	3.22±0.39	68±22	600±54	2.3±0.3
[FeX]	6376.00	1.83±0.19	5.44±0.56	−160±36	1301±94	3.9±0.4

Note that while some of the UV flux measured by *Swift* contains a contribution from extended star-formation (detected in the UV out to a radius of 15 arcsec), the fact that it is variable, and brighter than the archival *GALEX* UV central flux indicates that it is associated with the transient. The UV-optical color of ZTF18aajupnt/AT2018dyk after subtracting off the *GALEX* flux is UVW2−r = −0.45 mag, very similar to iPTF16bco (which had NUV−r = −0.5 mag, already 0.5 mag bluer than the color range of AGN in both

GALEX and SDSS; Bianchi et al. (2005); Agüeros et al. (2005)).

We obtained UV spectroscopy of ZTF18aajupnt/AT2018dyk with the Space Telescope Imaging Spectrograph (STIS) FUV and NUV Multi-Anode Microchannel Array (MAMA) detectors aboard the *Hubble Space Telescope* (*HST*) for a 2 ks exposure with 0″2 slit width, and G140L (λ = 1425 Å) and G230L (λ = 2376 Å)
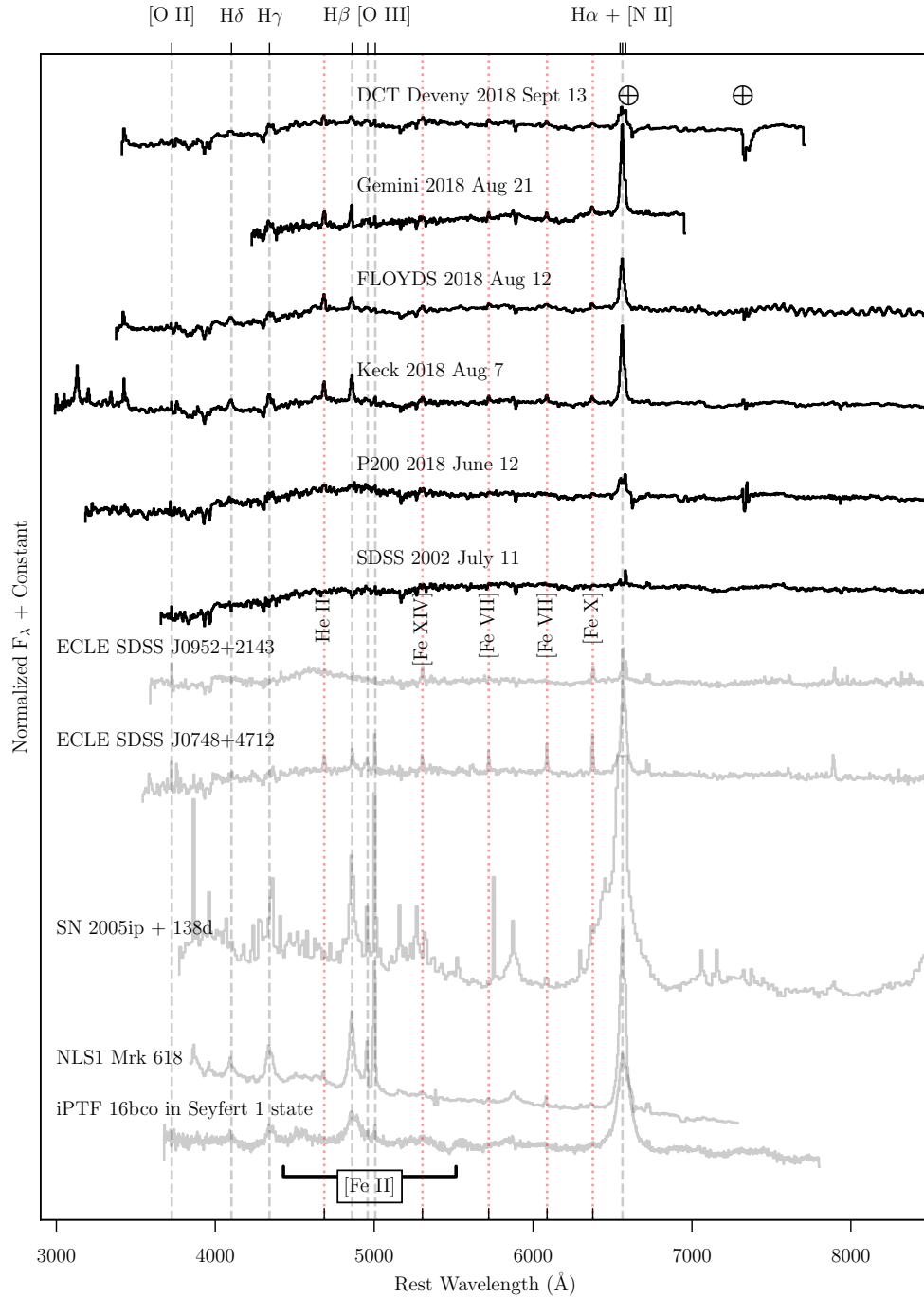
Figure 6. Host and follow-up spectra of ZTF18aajupnt/AT2018dyk, alongside various AGN and coronal line emitters for comparison. AGN emission lines are annotated in gray and are labeled above the figure. Coronal lines are annotated in red and are labeled in the middle of the figure. The flux of the Hα line (only) in SN 2005ip has been truncated for visual purposes (as it lies well above the upper boundary of the plot). Spectra have been rebinned by a factor of four for visual purposes.

gratings on 2018 Sept 1, 2019 Jan 18 (only in the FUV[7]),

and 2019 March 3, shown in Figure 9 (Proposal ID: 15331, PI: S.B. Cenko).

The high spatial resolution of *HST* ($\sim 0\rlap{.}''5$) enables better isolation of the nuclear emission from the host galaxy light. The UV continuum, when masking the emission lines and correcting for Galactic extinction as in Section 7, is an
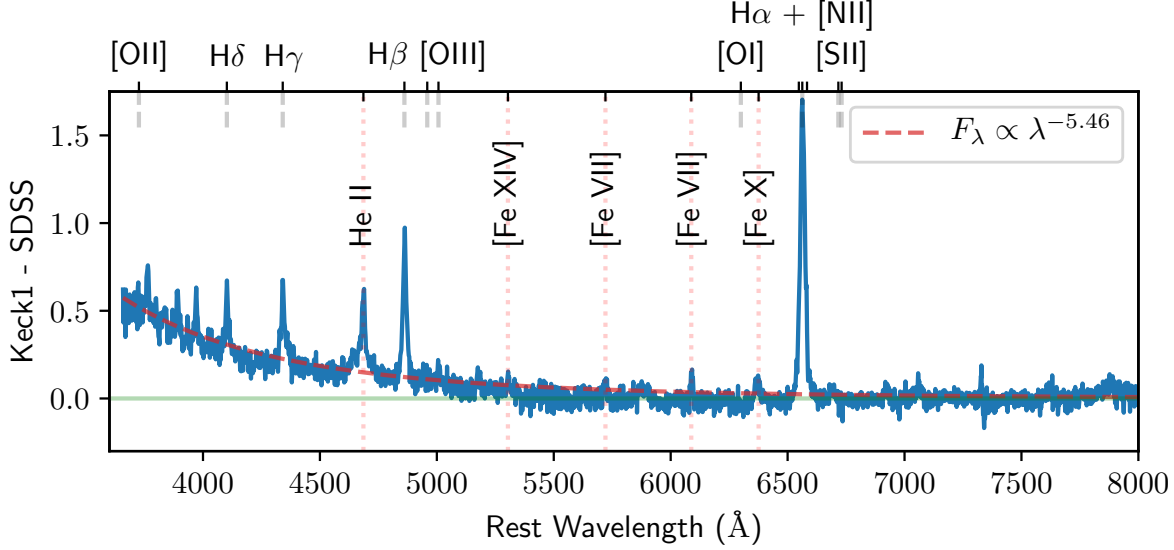
Figure 7. Host-galaxy-subtracted Keck1 spectrum of ZTF18aajupnt/AT2018dyk showing presence of coronal emission lines (red dotted lines) and a blue excess in the residuals. We fit the non-stellar blue continuum with a power law (red dashed line with $\alpha = -5.46$).
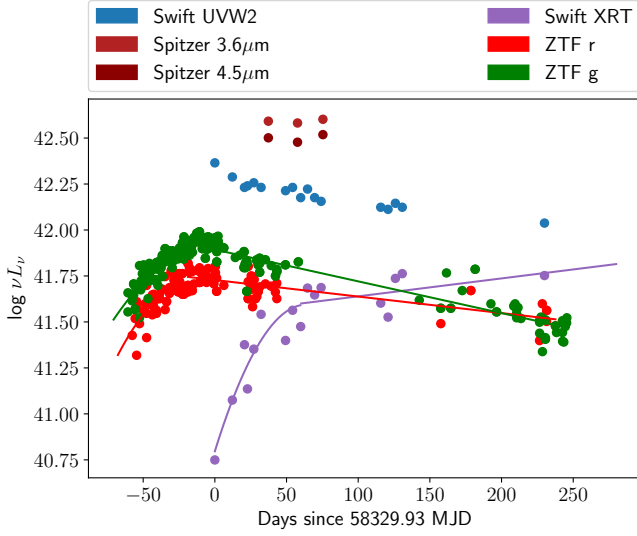
Figure 8. The νL_ν light curve of ZTF18aajupnt/AT2018dyk, comparing *Spitzer* data to concurrent *Swift* UVOT, XRT and ZTF observations. For the *Spitzer* and *Swift* UVOT observations we subtracted the host galaxy light as estimated by WISE and *GALEX* measurements, respectively. To better show the 60-day lag in the X-ray, we fit the rise caught by optical and X-ray observations with an order 2 polynomial and the plateau with linear fits.

equally good fit to both a blackbody (remaining consistent for both observations within T= $(4.5 \pm 0.3) \times 10^4$ K) and a power law with spectral index $\alpha = -2.6 \pm 0.1$ where $F_\lambda = F_{\lambda,0} \lambda^\alpha$ or $\alpha_\nu = -\alpha - 2 = 0.6$, with the continuum $F_{\lambda,0}$

decreasing in flux by a factor of 10.7 over 140 days, while the strength of the emission lines remain roughly at the same level. This blackbody temperature is not unusual for TDEs (e.g. van Velzen et al. 2011; Gezari et al. 2012; Arcavi et al. 2014; Holoien et al. 2016b,a; Hung et al. 2017), and the power-law index is within the range of UV slopes observed in quasars ($-1.5 < \alpha_\nu < 1.5$; Davis et al. 2007), but steeper than the UV slopes observed in NLS1s ($-2 < \alpha_\nu < 0$; Constantin & Shields 2003). Figure 9 shows similarities of the emission features to *HST* Faint Object Spectrograph (FOS) spectra of the prototypical NLS1s Mrk 335 and Mrk 478, noting that compared to the NLS1s, the UV spectrum of ZTF18aajupnt/AT2018dyk initially has a weaker low-ionization line Mg II $\lambda2798$, which tends to exhibit weak responsivity in CLAGN (e.g. MacLeod et al. 2016; Gezari et al. 2017). In the latest *HST*/STIS epoch, ∼6 months after the optical peak, a broad multi-component Mg II line profile appeared, reminiscent of recently "awakened" CLAGN Mrk 590 (Mathur et al. 2018). This suggests that a light travel time delay, and not low responsivity, is responsible for Mg II being only marginally detected in the intial observation. This also implies that Mg II is not co-spatial with the Balmer-line emitting region.

Galactic extinction has been corrected in these spectra in the same way as in Section (7), but instead using the UV correction curve for $R_V = 3.1$ given by Eqs. 4.a. and b. in Cardelli et al. (1989).

2.7. X-ray

We observed ZTF18aajupnt/AT2018dyk concurrently with 17 exposures of *Swift* XRT, detailed in Table 5. The
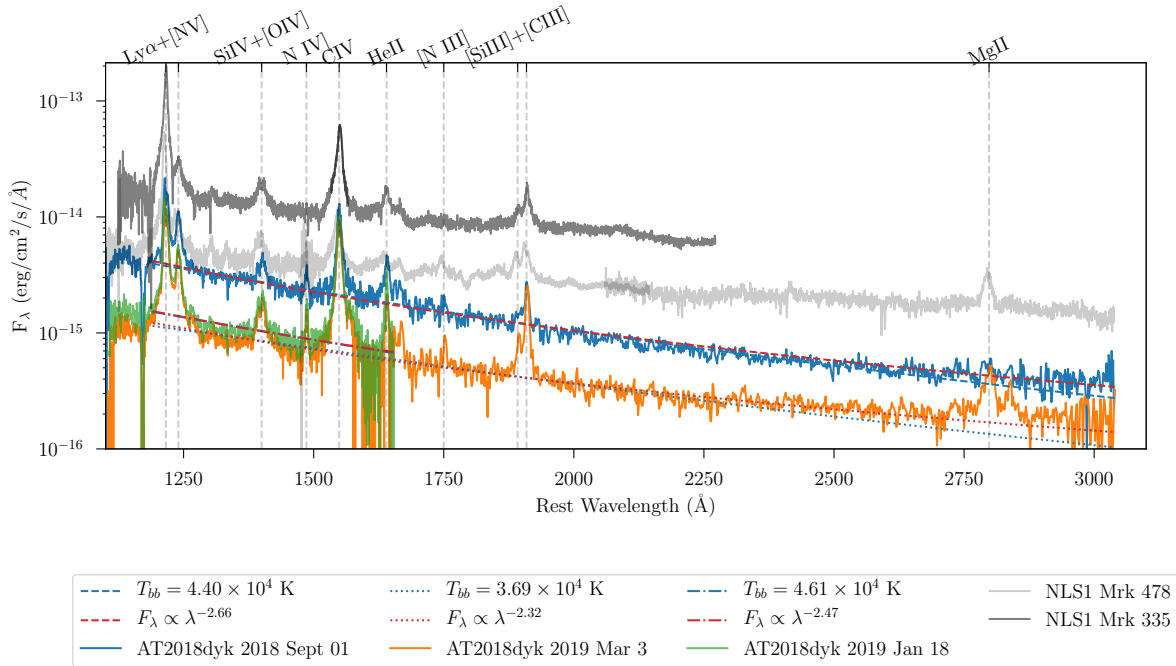
Figure 9. *HST* UV spectrum of ZTF18aajupnt/AT2018dyk compared to two prototypical NLS1s. Note the presence of high-ionization lines He II, N V, O IV, and C IV, and the relative weakness of the low-ionization line Mg II $\lambda2798$ in ZTF18aajupnt/AT2018dyk until later times.

XRT data were processed by the XRT Products Page[8] (Evans et al. 2009) using HEASOFT v6.22[9]. We assessed best-fit models utilizing χ^2 statistics and XSPEC version 12.9.1a (Arnaud 1996). Uncertainties are quoted at 90% confidence intervals. The XRT light curve in the lower panel of Figure 10 shows that ZTF18aajupnt/AT2018dyk is a strongly variable X-ray source, caught rising steadily by an order of magnitude in flux over several months. The coadded spectrum (shown in the upper panel of Figure 10) is well-modeled by a power law with a spectral index of $\Gamma = 2.82^{+0.35}_{-0.26}$ and assuming a Galactic extinction of $N_{\rm H} = 1.76 \times 10^{20}$ cm^{-2} (computed by the `NHtot` tool; Kalberla et al. (2005); Schlegel et al. (1998)), with no intrinsic absorption and an observed flux between 0.3–10 keV of $(3.0\pm0.5) \times 10^{-13}$ erg cm^{-2} s^{-1}.

We then observed ZTF18aajupnt/AT2018dyk with the *XMM* EPIC pn camera (Strüder et al. 2001) on 2018 Aug 11 for a 12 ks exposure (Observation ID: 0822040701, PI: S. Gezari). We reduced the data using the *XMM-Newton* Science Analysis System (SAS) v16.0 (Gabriel et al. 2004). We extracted products with circular source and background (source-free) regions with radii of 35" and 108", respectively. To mitigate background flaring and maximize SNR, we filtered the photometry for count rates below 1.75 cts s^{-1}. We also adopted CCD event patterns 0 to 4,

corresponding to single- and double-pixel events. We used *XMM Newton* EPIC-pn calibration database files updated as of Sept 2018. We fit the *XMM* EPIC pn data to a simple power law with spectral index $\Gamma = 3.02 \pm 0.15$ and only Galactic extinction, characteristic of a steep soft excess, and consistent with the range of photon indices observed for NLS1s ($\overline{\Gamma} = 2.8 \pm 0.9$; Boller et al. 1996; Forster & Halpern 1996; Molthagen et al. 1998; Rakshit et al. 2017).

Using the PIMMS count rate calculator[10], the conversion factor between counts and unabsorbed flux is 3.1×10^{-11} for XRT, and 1.5×10^{-12} for *XMM*.

2.8. *Infrared*

Spitzer Infrared Array Camera (IRAC; Fazio et al. 2004) observations were triggered for five epochs on 2018 Aug 13 under the approved ToO program (PI: Yan, PID:13251). At each epoch, the data were taken for both 3.6 and 4.5μm, each with a total of 600 seconds exposure time. A 50 point cycling dither pattern was used. The first three epochal data were taken and used for the analysis when this paper was prepared. The coadded and mosaiced images were produced by the standard *Spitzer* pipeline and are directly used by our analysis.

We measured a maximum increase of 0.14 mag compared to archival WISE observations. We correct the difference magnitude for the small difference between the bandpass of

Table 5. *Swift UVOT/XRT* photometry for ZTF18aajupnt/AT2018dyk. Corresponds to lower panels of Figures 10 and 11.

Obs UT	*UVOT/XRT* Exposure times (s)	Count rate $(10^{-2}\ s^{-1})$	UVW2 (AB mag)	Unabsorbed $F_{0.3-10keV}$ $(10^{-13}\ erg\ s^{-1}\ cm^{-2})$	$L_{2\ keV}$ $(10^{40}\ erg\ s^{-1})$	$L_{2500\ A}$ $(10^{42}\ erg\ s^{-1})$	α_{OX}
2018 Jul 30	931/941	0.4 ± 0.3	17.72 ± 0.04	1.21	0.56	6.80	-1.15
2018 Aug 12	312/2022	0.8 ± 0.3	17.90 ± 0.06	2.64	1.19	5.70	-1.00
2018 Aug 20	491/3001	1.7 ± 0.3	18.05 ± 0.05	4.43	2.38	5.00	-0.86
2018 Aug 22	298/2252	1.0 ± 0.2	18.03 ± 0.06	2.55	1.37	5.10	-0.96
2018 Aug 27	375/3164	1.6 ± 0.3	17.99 ± 0.06	4.18	2.25	5.30	-0.88
2018 Sep 01	286/2874	2.4 ± 0.3	18.05 ± 0.06	6.48	3.48	5.00	-0.80
2018 Sep 18	807/3006	1.7 ± 0.3	18.10 ± 0.05	5.43	2.51	4.80	-0.85
2018 Sep 23	165/3011	2.5 ± 0.3	18.05 ± 0.08	7.93	3.66	5.00	-0.79
2018 Sep 28	324/1877	2.1 ± 0.4	18.20 ± 0.06	6.47	2.98	4.40	-0.80
2018 Oct 03	353/3149	3.4 ± 0.4	18.08 ± 0.06	10.47	4.83	4.90	-0.74
2018 Oct 08	582/2447	3.1 ± 0.4	18.18 ± 0.05	9.60	4.43	4.40	-0.74
2018 Oct 13	1677/1695	3.4 ± 0.5	18.23 ± 0.04	10.53	4.86	4.20	-0.71
2018 Nov 23	1329/2931	2.8 ± 0.3	18.33 ± 0.05	8.68	4.00	3.90	-0.73
2018 Nov 28	1380/2854	2.3 ± 0.3	18.36 ± 0.05	7.27	3.36	3.80	-0.76
2018 Dec 03	1281/2484	3.8 ± 0.4	18.28 ± 0.05	11.82	5.46	4.10	-0.69
2018 Dec 08	629/2452	4.0 ± 0.5	18.33 ± 0.05	12.54	5.79	3.90	-0.67
2019 Mar 17	191/2874	3.9 ± 0.4	18.55 ± 0.09	12.24	5.65	3.20	-0.64

the two instruments: 0.19, 0.03 mag for channels 1 and 2, respectively, as measured using stars in the field. In Figure 8, we show that this νL_ν at 3.6/4.5 μm (subtracting our estimate of the host galaxy baseline as measured by WISE) is greater than νL_ν in the UV, suggesting a large dust covering factor (the fraction of solid angle from the central source obscured by dust).

NEOWISE data (WISE, Wright et al. 2010) showed there was no variability from the host galaxy of ZTF18aajupnt/AT2018dyk for 1 year prior to its discovery in ZTF, despite the hint of optical variability observed in June 2016 by iPTF (Section 2.2).

2.9. *Radio*

We measure an archival FIRST VLA survey intensity upper limit (including CLEAN bias) of 0.89 mJy beam^{-1} at the location of the host of ZTF18aajupnt/AT2018dyk in 1997.

3. ANALYSIS

3.1. *Host Galaxy Classification*

We compare the SDSS spectra of the LINER hosts, observed more than a decade prior to the changing looks caught by ZTF, with follow-up observations taken using the Palomar 60-inch (P60) telescope and the DCT in Figure 4. We fit stellar absorption and narrow emission lines to the host spectra with pPXF and results are in Figure 12. To distinguish them from star-forming galaxies, Kauffmann

et al. (2003) define a galaxy as a Seyfert if

$$\log([OIII]/H\beta) > 0.61/(\log([NII]/H\alpha) - 0.05) + 1.3.$$

and Kewley et al. (2001) demarcate a Composite galaxy if

$$0.61/(\log([NII]/H\alpha) - 0.47) + 1.19 < \log([OIII]/H\beta)$$

is true. These functions are represented as the dashed and solid lines (respectively) in the BPT [OIII]/Hβ versus [NII]/Hα narrow-line diagnostic diagram shown in the upper left panel of Figure 13. Figure 13 also shows various other line ratio diagnostic diagrams involving the line ratios [OIII]/Hβ, [NII]/Hα, [OI]/Hα, and [OIII]/[OII] (Baldwin et al. 1981; Kewley et al. 2001, Kauffmann et al. (2003), Kewley et al. 2006), including the WHAN diagram (Cid Fernandes et al. 2011), accounting for the equivalent width of Hα and the fact that the typical BPT LINER classification contains both "weak AGN" and "retired galaxies" that have ceased star formation.

Analysis of the archival SDSS spectra of the individual sources in this sample finds that all but CLQ iPTF16bco exist in the borderline region between LINER and Seyfert classifications for all five diagnostics shown in Figure 13. According to the diagram of Cid Fernandes et al. (2011), both weak and "fake" AGN scenarios are plausible within the 1σ errorbars for three LINERs in this sample, excluding the host of iPTF16bco, which is considered a retired galaxy in this diagnostic, and the hosts of ZTF18aasszwr and ZTF18aaabltn, which are Seyfert-like (see lower left panel of Figure 13).
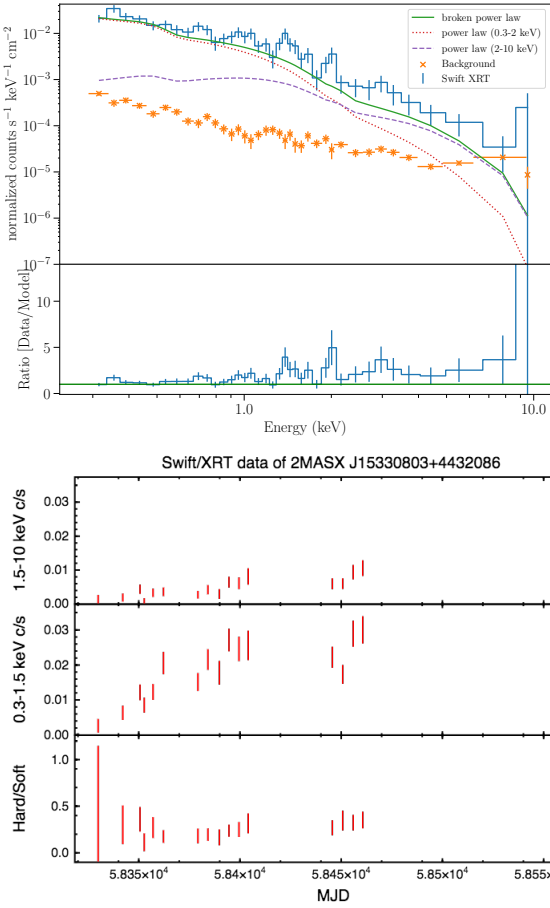
Figure 10. Upper panel: XRT spectral fit to a broken power law with soft photon index $\Gamma = 2.82^{+0.35}_{-0.26}$ described in Section 3.6.4. Lower panel: Although a slow rise is evident at the 0.01 counts s^{-1} level in the hard band (defined as 1.5–10 keV), the hardness ratio light curve shows that the X-ray flare is primarily soft, i.e. 0.3–1.5 keV.

We note that the broad Hα component of ZTF18aaabltn is not completely gone in the spectrum representing its "off" state. Although it passed the sample selection criteria of being identified as a LINER in the Portsmouth SDSS DR12 catalog (described in Section 2.1), re-fitting of the line ratios of ZTF18aaabltn reveals that it is a Seyfert rather than a LINER. As we measured a broad base in Hα, we classify it instead as a Sy 1.9 (this is also consistent with prior radio and X-ray detections of this source). ZTF18aasuray displayed double-peaked broad Balmer emission indicative of an persistent broad line region with unchanging kinematics in both its low and high states. As the peaks did not represent high enough velocities or asymmetric enough profiles to require separate components, we fit a single broad Gaussian base in this source when measuring the narrow line ratios. Unlike ZTF18aaabltn, those measurements were in agreement with the LINER classification.
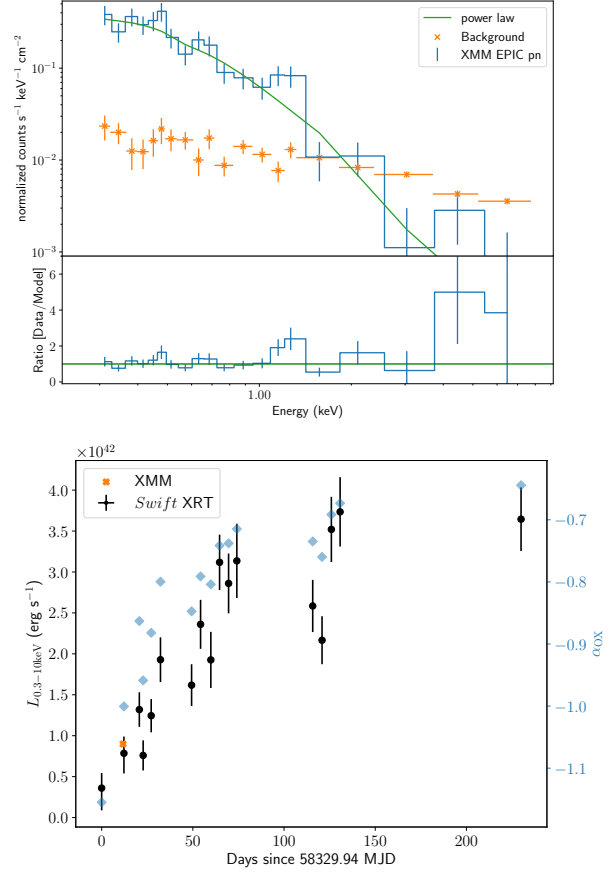

Figure 11. Upper panel: The *XMM* EPIC pn data of ZTF18aajupnt/AT2018dyk fit to a simple absorbed power law with spectral index $\Gamma = 3.02 \pm 0.15$ shows a prominent, steep soft excess. Lower panel: The X-ray luminosity derived from a power law fit with $\Gamma = 3$ is plotted in comparison with $\alpha_{\rm OX}$ (described in Section 3.6.4).

Similarly to this work, Thomas et al. (2013) also used pPXF to fit stellar kinematics and the [S II]/Hα ratio diagnostic from Schawinski et al. (2007) (upper right panel of Figure 13) to classify a source as a LINER; however, they used the Gas and Absorption Line Fitting code (GANDALF v1.5; Sarzi et al. (2017)) to fit emission lines, whereas we use a simple multi-component Gaussian profile fit to the narrow lines in the stellar-template-subtracted spectra (see Figure 18 in the Appendix for these model fits). There may also be a discrepancy stemming from GANDALF correcting for dust—the majority of this sample have Balmer decrement $f_{\rm H\alpha}/f_{\rm H\beta} > 3.1$, indicative of strong intrinsic reddening. However, we choose not to apply a dust correction since it is an uncertain measurement for this sample, due to the weak emission line intensities.

3.2. *Black Hole Masses*

In order to shed light on the physical differences between the individual AGN in this sample, we estimate the black hole masses of the CLAGN hosts using several methods.
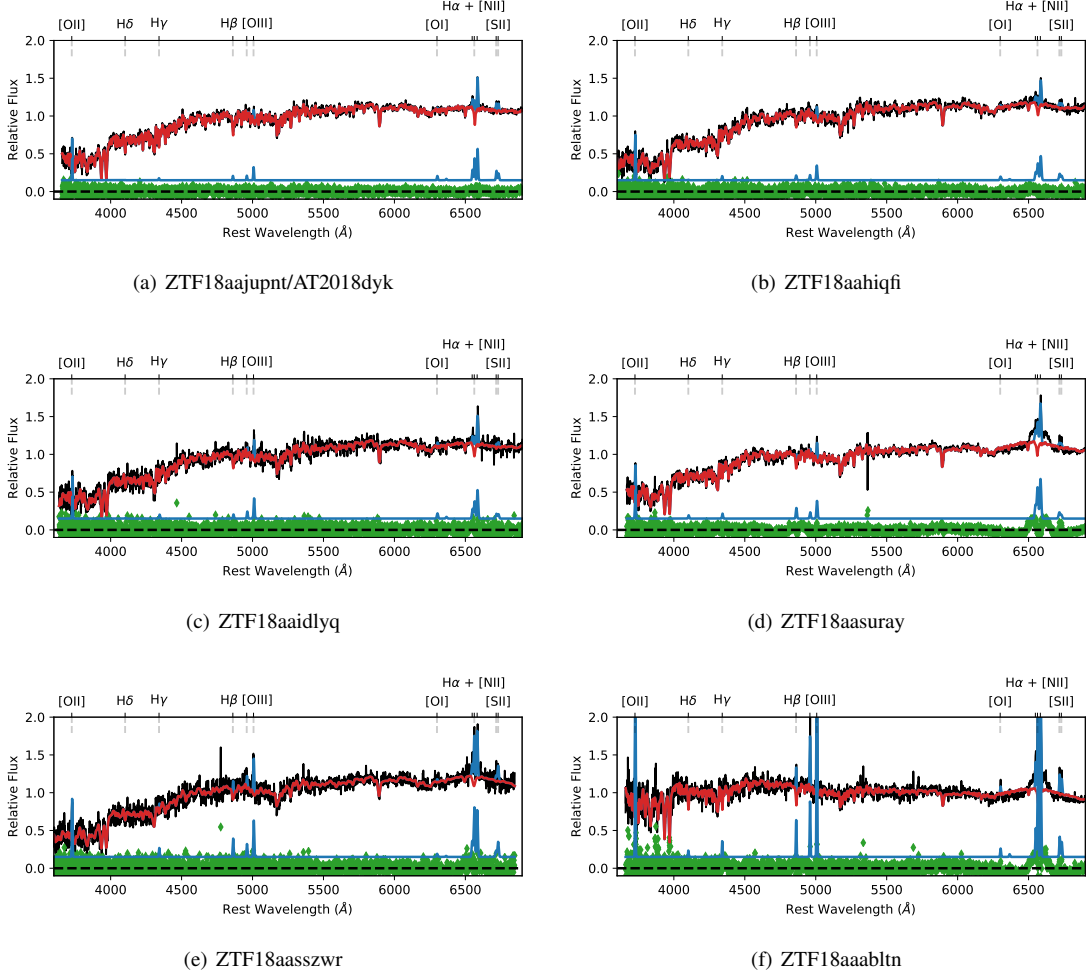
Figure 12. The SDSS spectra of the host galaxies were fit using the Penalized Pixel-Fitting (PPXF) method by Cappellari & Emsellem (2004). Red denotes the stellar population template, blue the emission line fits, and green points the residuals to the total best fit model. Note the poor fit to the [O II] and [O III] emission lines of ZTF18aaidlyq, which are replaced in subsequent analysis by the emission line fits in Figure 18. We do not re-analyze iPTF16bco (not shown here) and instead use the analysis from Gezari et al. (2017).

The broad Hβ line is the most common virial estimator for BH masses at low redshift ($z \lesssim 0.4$; e.g. Marziani & Sulentic 2012).

$$M_{\rm BH,vir} = 1.5 \times 10^5 \left(\frac{R_{\rm BLR}}{\text{light days}} \right) \left(\frac{\text{FWHM}(\text{H}\beta)}{10^3 \text{kms}^{-1}} \right)^2 M_\odot$$

where $R_{\rm BLR} = 32.9 (\frac{\lambda L_{5100A}}{10^{44} \text{ergs}^{-1}})^{0.7}$ light days (Kaspi et al. 2000). We also calculate $M_{\rm BH}$ from the host galaxy luminosity following McLure & Dunlop (2002) such that

$$M_{\rm BH,M_r} = -0.5 M_{r,\text{host}} - 2.96,$$

and the host bulge stellar mass using the relation from Häring & Rix (2004)

$$\log(M_{\rm BH,Bulge}[M_\odot]) = \log(0.0014 M_{\rm Bulge}[M_\odot]),$$

and computed and from the stellar velocity dispersion ($\sigma_\star$) measured from the SDSS spectrum using the pPXF method) using the $M_{\rm BH} - \sigma$ relation from Tremaine et al. (2002)

$$\log M_{\rm BH,\sigma\star}[M_\odot] = 8.13 + 4.02 \log(\sigma_\star / 200 \text{ km s}^{-1}).$$

The results of these measurements are summarized in Table 2, and discussed further in Section 3.3.

3.3. *Comparison to Tidal Disruption Events*

It is important to compare the properties of this class of AGN "turning-on" from quiescence with a related phenomenon of tidal disruption events (TDEs). When a star passes close enough to a central black hole to be ripped apart by tidal forces, roughly half of the stellar debris will remain bound to the black hole and provide a fresh supply of gas to accrete onto the black hole. The evolution of the flare of radiation from a TDE is regulated by the fallback
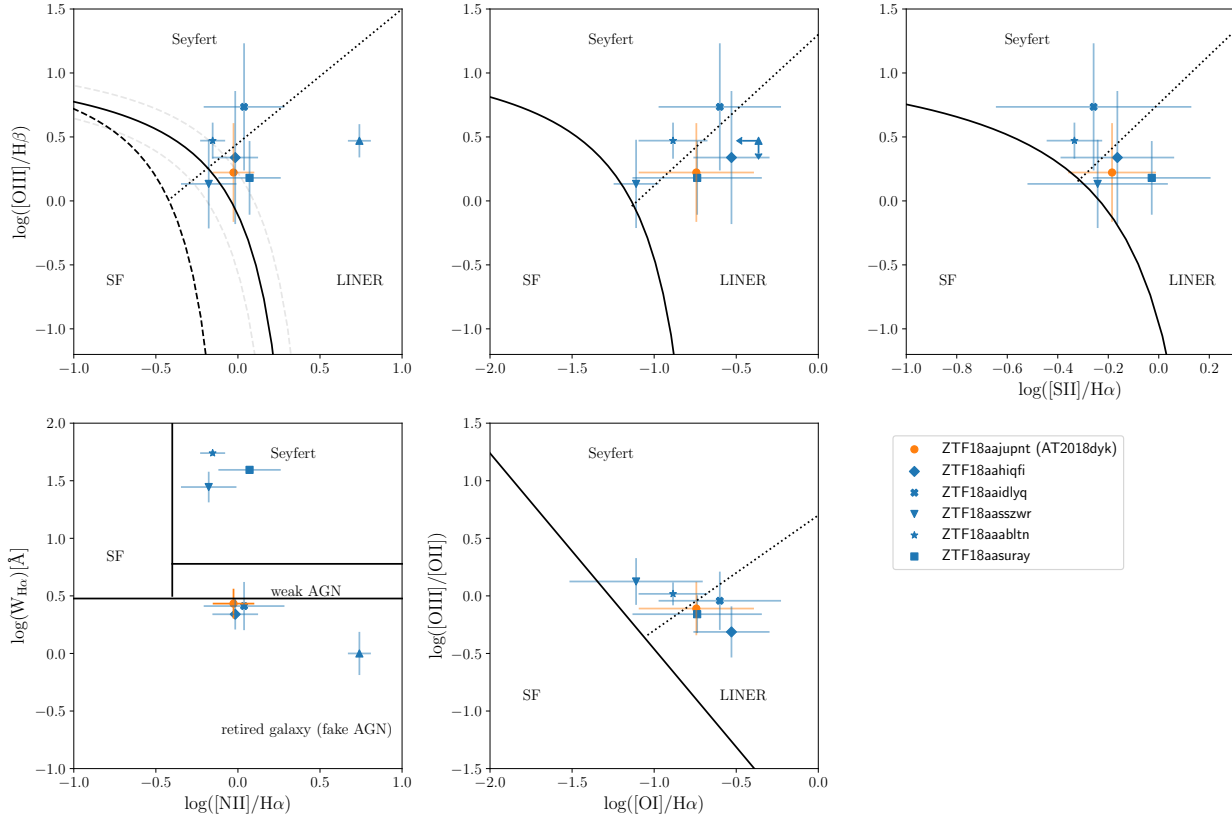
Figure 13. Narrow-line diagnostics for the CL LINER sample in the "off" state (i.e. their host galaxies), including iPTF16bco (values from Gezari et al. (2017)). The majority of the sample is on the borderline between a LINER and Seyfert classification. Note differences in scale. Upper limits are used when lines are not significantly detected.

Lower left panel: AGN diagnostic diagram from Cid Fernandes et al. (2011). Only three of the sources in the CL LINER sample require a Seyfert to power the Balmer emission lines in their low state, also indicated by the Hα line profiles requiring broad components, shown in the fits in Figure 18.

timescale ($t_{\rm fb}$), the time delay for the most tightly bound debris to return to pericenter after disruption, and the circularization timescale, which is dependent on the efficiency at which the debris streams shock and circularize due to general relativistic precession. Interestingly, the virial black hole mass for all the CL LINERS in the iPTF/ZTF sample are above the black hole mass for which a solar-type star can be disrupted outside the event horizon ($M_{\rm BH} \lesssim 10^8 \ M_\odot$). The only exception is ZTF18aajupnt/AT2018dyk, which as a NLS1 in its "on" state, thus with narrower lines, naturally implies a smaller black hole mass with this method. However, the black hole mass inferred from the host galaxy velocity dispersion and bulge mass suggest a larger black hole mass of $\log(M_{\rm BH}/M_\odot) = 7.6 - 7.8$. This trend of the black hole mass from the virial method being much smaller is consistent with the work of Rakshit et al. (2017), who suggest that the smaller Balmer line widths measured in NLS1s which lead to lower BH masses are due to the geometrical effects of being viewed more face-on ($\langle i \rangle = 26°$) compared to normal broad line Sy 1s ($\langle i \rangle = 41°$). This claim is backed up by spectropolarimetric studies of NLS1s (Baldi et al. 2016),

Alternately, Marconi et al. (2008) suggested that in rapidly accreting objects (including NLS1s), enhanced ionizing radiation pressure could also lead to underestimates of virial black hole mass estimates.

It is also possible that these transitioning AGN do not obey the radius-luminosity relation established from reverberation mapping studies of Seyfert galaxies. If we instead use the black hole mass estimates from the host galaxy velocity dispersion, luminosity, and/or stellar mass, we find that the CL LINER sample have black hole masses of $\log(M_{\rm BH}/M_\odot) \sim 7 - 8$, close to, but not necessarily exceeding the upper mass limit for the tidal disruption of a solar-type star.

We can also compare the light curves and spectra of our CL LINERs to TDEs. The quiescence in the light curves before the onset of their flaring activity, their blue colors ($g - r < 0$) during the flaring in most of the cases, as well as their smooth decline from peak are generally consistent with the TDE scenario. The main distinction is in their spectral properties at peak. The five objects caught transitioning from a LINER to a type 1 AGN show spectra in their "on" state that are almost indistinguishable from normal quasars,

besides the relative weakness of [O III]. In contrast, TDEs exhibit exclusively broad emission lines; broad He II $\lambda4686$ emission, and/or broad Hα and Hβ lines, and sometimes broad He I, but with line luminosities of $\lesssim 10^{41}$ ergs s^{-1} (Arcavi et al. 2014; Brown et al. 2016; Hung et al. 2017; Holoien et al. 2018), well below the CL LINERs (see Figure 14). Furthermore, the X-ray spectra of the CL LINERs with X-ray observations in their "on" state, iPTF16bco and ZTF18aajupnt/AT2018dyk, are well described by a power-law, with $\Gamma = 2.1$ (Gezari et al. 2017) and $\Gamma = 3.0$, respectively, and are clearly distinct from the extremely soft blackbody spectra with $kT \sim 0.04-0.10$ keV characteristic of both optically and X-ray selected TDEs (Komossa 2002; Miller et al. 2015; van Velzen et al. 2019). We present a more detailed comparison of the observed properties of ZTF18aajupnt/AT2018dyk with TDEs in Section 3.6.

3.4. *Comparison to Seyfert CLAGN*

We measure the Hα and [O III] $\lambda5007$ luminosities for this sample in their "on" state in Figure 17 and compare to that of SDSS Sy 1s (including NLS1s; Mullaney et al. (2013)) and quasars (Shen et al. 2011). All AGN in this sample display [O III] $\lambda5007$ luminosities significantly below average for their observed broad Hα luminosity in their "on" state, consistent with the findings of Gezari et al. (2017), that CLQs with appearing (disappearing) broadlines were in general closer to the fringe (average) of the quasar distribution. However, for ZTF18aasszwr and ZTF18aaabltn, only upper limits of [O III] were possible due to the low SNR for narrow lines of the low-resolution ($R \sim 100$) follow up spectra.

MacLeod et al. (2019) systematically obtained spectra for highly-variable candidate CLQs (defined as type 1 AGN transitioning to type 2s or vice versa) within the SDSS footprint, requiring Pan-STARRS 1 variability exceeding $|\Delta g| > 1$ mag and $|\Delta r| > 0.5$ mag. We find agreement with their measured positive correlation between broad emission line and continuum flux changes, but find that our sample of CL LINERs is more extreme in the parameter space of continuum and Hβ flux ratios (ranging from 2−800 and 12−400, respectively) than the CLQ sample from MacLeod et al. (2019) (with $f_{\rm high}/f_{\rm low} = 1-7$ and 2−8 for continuum and Hβ, respectively), shown in Figure 14. When restframe flux at 3240 Å was not available to us due to inconsistent spectral coverage, we measured flux at the shortest available comparable wavelength.

3.5. *Eddington Ratio Estimates*

We compute the Eddington ratio ($L_{\rm bol}/L_{\rm Edd}$) for the sample in their "on" state assuming $L_{\rm bol} = 9\lambda L_{5100A}$ (Kaspi et al. 2000), summarized in the final column of Table 2. $L_{\rm bol}$ in the "on" state is measured using difference imaging in the filter with central wavelength closest to rest-frame 5100 Å for each source (r-band for higher-redshift sources iPTF16bco, ZTF18aaidlyq, and ZTF18aasszwr, and g-band for all others). $L_{\rm bol}$ in the "off" state is measured from the

reddening corrected $L_{\rm [O III]}$ narrow line luminosity correlation to $L_{2-10 \rm keV}$ for type 2 AGN (Equation 1 in Netzer et al. (2006)) and using the same bolometric correction as Elitzur et al. (2014), $L_{\rm bol} = 15.8L_X$.

While virial black hole masses based on the broad Hβ line and continuum luminosity are more generally used for AGN, those relations are based on reverberation mapping studies which were never done specifically for NLS1s. Thus, for the remainder of this work, we adopt BH mass estimates for the sample to be consistent with $M_{\rm BH}$ from stellar velocity dispersions as described in Section 3.2 and summarized in Table 2.

The Seyfert CLAGN with appearing broad emission lines in the variability-selected MacLeod et al. (2019) sample (summarized in Section 3.4) have $-2 \lesssim \log(L/L_{\rm Edd}) \lesssim -1$, slightly below that of a control sample of extremely variable quasars and normal SDSS DR7 quasars. For the relatively large range of this small sample ($-1.7 \lesssim \log(L/L_{\rm Edd}) \lesssim -0.3$), it is difficult to distinguish which population's Eddington ratios to which they are better matched in their "on" state. The corresponding upper limits of $\log(L/L_{\rm Edd}) < -2$ in the "off" states of the LINER host galaxies are in good agreement with that of the MacLeod et al. (2019) CL population that has dimmed.

Elitzur et al. (2014) predict a natural sequence within the disk-wind scenario in which AGN evolve from displaying to lacking broad optical emission lines. This evolution is driven by variations in accretion rate (with the critical value parameterized by $L_{\rm bol}/M_{\rm BH}^{2/3}$), as well as the availability of ionizing radiation from the central engine. The BLR is therefore posited to be assembled following an increase in accretion rate (likely due to instabilities to match the fast timescales observed; Rumbaugh et al. (2018)). Due to an insufficient cloud flow rate and lack of ionizing photons, no BLR can be sustained below the critical accretion rate or bolometric luminosity ($L_{\rm bol} \leq 5 \times 10^{39}M_7^{2/3}$ erg s^{-1}, Elitzur & Ho (2009)). This spectral evolutionary pathway is supported by modeling an SDSS-selected sample of Seyferts of various types and spanning $L/L_{\rm Edd} \sim 10^{-3}$ to 0 (Stern & Laor 2012), for which accretion rate progressively decreased with luminosity from type 1s to type 2-like AGN. In Figure 15 we recreate this sequence represented by AGN with different spectral classifications occupying distinct regions of the $L_{\rm bol} - M_{\rm BH} - L/L_{\rm Edd}$ parameter space and roughly separated by the critical threshold of Elitzur & Ho (2009). We overplot the CL LINER sample in their "on" states which overlap roughly with the Seyfert type 1 sources, and in the "off" LINER states which overlap largely with the type 2s and border on the intermediate type 1.2/1.5 Seyferts.

The bolometric luminosities (and therefore the Eddington ratios) are upper limits in Figure 15 due to the "off" spectra being almost entirely host dominated. iPTF16bco, ZTF18aasuray, ZTF18aaidlyq, and ZTF18aasszwr approach the quasars in their "on" states, and ZTF18aajupnt/AT2018dyk does not fall squarely among the NLS1s but instead in the border region between types. The
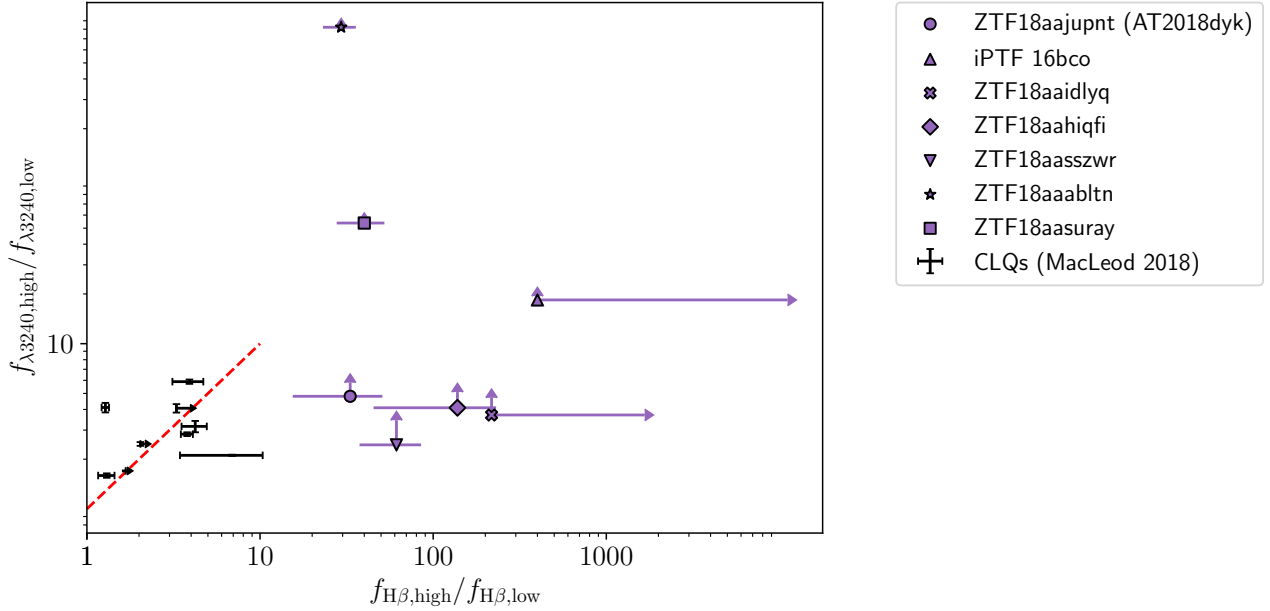
Figure 14. Ratio of continuum flux change as a function of broad line flux change for our changing look LINER sample (filled shapes) in comparison to changing look Seyferts. ZTF18aajupnt/AT2018dyk (purple circle), is intermediate in flux ratio and Hβ ratio space between Seyfert CLAGN (black, lower left) and the other CL LINERs in this sample. The red dotted line denotes a 1:1 ratio between the continuum and Hβ fluxes. iPTF16bco, ZTF18aasuray, ZTF18aasszwr, iPTF16bco are outliers in differential continuum space (although we collected spectra of the latter two with an IFU spectrograph that can be unreliable at bluer wavelengths), and iPTF16bco, ZTF18aaidlyq, and ZTF18aahiqfi are outliers in Hβ luminosity space compared to that of the Seyfert CLAGN. All have much larger (by a factor of > 10) changes in broad line flux than the changing look Seyfert sample. The $f_{\lambda 3240}$ ratio measurements are represented as lower limits, as there is stellar contamination in the low (LINER) state. Adapted from Figure 6 in MacLeod et al. (2019).

least luminous sources in the sample, ZTF18aajupnt/AT2018dyk and ZTF18aasuray, approach most closely the critical Eddington ratio for the existence of a BLR in their "off" states, and the most luminous iPTF16bco is closest to the intermediate types in its LINER state.

### 3.6. *ZTF18aajupnt/AT2018dyk: A LINER Changing-Look to a NLS1*

For the following analysis we focus on ZTF18aajupnt/AT2018dyk, for which we have the most extensive follow-up data, and which showed the appearance of coronal lines along with X-ray variability. The difference imaging light curve of this event displays a plateau similar to that of iPTF16bco (Gezari et al. (2017); see comparison in Figure 5), before fading gradually over several months in a manner similar to that of CL LINER ZTF18aasszwr, rather than the power-law decline characteristic of an optical TDE light curve (e.g. Hung et al. 2018).

The lack of IR variability in NEOWISE leading up to the turn-on of ZTF18aajupnt/AT2018dyk constrains the presence of any IR AGN activity or dust echo in this host to < 10 months. W1-W2 is never greater than ~ 0.02 during this time, far below the 0.8 threshold AGN diagnostic value from Stern et al. (2012). Stability in the CRTS light curve similarly confirms that no AGN-like variability was present

for 13 years prior to its discovery with ZTF. There was, however, a hint of some ~ 0.1 mag flaring in the CRTS light curve in June 2006 and April 2007. Additionally, we extracted forced photometry (Masci et al. 2017) for ZTF18aajupnt/AT2018dyk from the PTF database covering June 2011 to June 2016, and there were only 8 marginal detections near the limiting magnitude of PTF (from 20 to 20.9 r-band mag) for the last 15 days of this range.

To reproduce the photometry of ZTF18aajupnt/AT2018dyk, any physical explanation must explain a rise time of ~ 50 days and a slow decline rate of ~ 0.5 mag in 60 days, both quite unusual for a TDE or supernova (e.g. van Velzen et al. 2019). Arcavi et al. (2018) note that the difference imaging light curve of ZTF18aajupnt/AT2018dyk peaks at an absolute magnitude of -17.4 mag, which is much fainter than the majority of TDEs by several magnitudes, excluding iPTF16fnl (Blagorodnova et al. 2017). A power law and blackbody give nearly identical fits to the UV spectra (with $\overline{T_{\rm bb}} = 4.5 \times 10^4$ K) with no change in the slope as the continuum fades over ~ 140 days; Figure 9). The optical continuum in Figure 7 is well fitted with a power-law, consistent with the Rayleigh-Jeans tail of a blackbody.

In the UV, the observed spectrum does not resemble that of a TDE in a LINER (e.g. ASASSN-14li, Cenko et al.
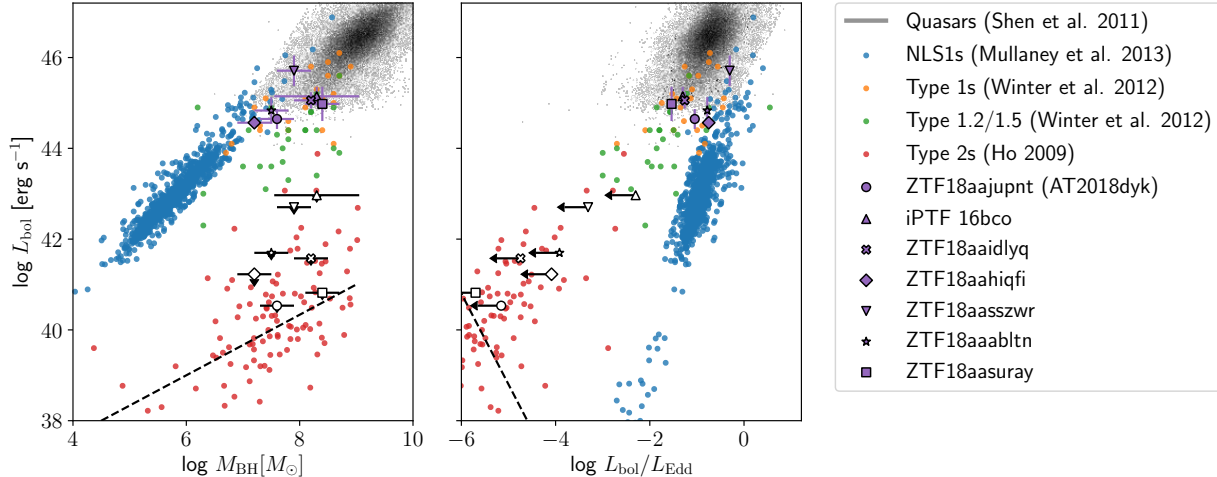
Figure 15. AGN, when separated by spectral classification, show the rough evolutionary sequence in parameter space of black hole mass M_{BH}, bolometric luminosity L_{bol}, and Eddington ratio $L_{\mathrm{bol}}/L_{\mathrm{Edd}}$ described in Section 3.5. The dotted lines denote the critical values above which a BLR can be sustained from Elitzur & Ho (2009) described in Section 3.5, to which we compare the measured values for the sample (filled, purple shapes with same mapping as in Figure 14) and their hosts (unfilled, black). The CL LINER sample in their "on" state is consistent with the type 1s (orange points), with ZTF18aajupnt/AT2018dyk in its high state (filled circle) toward the high luminosity end of the NLS1 distribution (blue points). We note that the type 2 sample from Ho (2009) contains LINER2s and LLAGN. Adapted from Figure 1 in Elitzur et al. (2014).

(2016)). Instead, the UV spectrum of ZTF18aajupnt/AT2018dyk is very similar to the UV spectra of normal NLS1s, with a similar spectral slope and peaked, broad emission line shapes (see Figure 9). In particular, ZTF18aajupnt/AT2018dyk has a strong C IV $\lambda\lambda1548, 1551$ line and C III] $\lambda1909$ line, which is typical of NLS1s, but not detected in all the TDEs with HST UV spectra: ASASSN-14li (Cenko et al. 2016), iPTF15af (Blagorodnova et al. 2018a), iPTF16fnl (Brown et al. 2018), AT2018zr (Hung et al. 2019). Interestingly though, ZTF18aajupnt/AT2018dyk does show N IV] $\lambda1486$ emission, which is just barely detected in NLS1s (Constantin & Shields 2003) and *is* detected in the UV spectrum of TDE ASASSN-14li, which was argued to be N-rich. The critical density 3.4×10^{10} cm^{-3} of the intercombination N IV] $\lambda1486$ line provides an upper limit to the density of this gas in ZTF18aajupnt/AT2018dyk (Nussbaumer & Storey 1979). The late-time increase in the Mg II line has not been detected in a TDE; in fact the opposite trend has potentially been observed: the brightening of broad Mg II with the fading of the transient in TDE AT2018zr (Hung et al. 2019). Finally, ZTF18aajupnt/AT2018dyk demonstrates none of the broad absorption features seen in the UV spectra of TDEs, and has been associated with powerful outflows launched by the accretion process in a TDE.

3.6.1. *Coronal Line Emission from ZTF18aajupnt/AT2018dyk*

We report line measurements of the Keck spectrum of ZTF18aajupnt/AT2018dyk in Table 4. We choose to analyze the spectrum from this instrument because of its sufficiently

high SNR and spectral resolution to measure the presence of coronal lines. For each of these measurements, the stellar population of the host galaxy represented by the ppxf fit has been subtracted (See Figure 12 for a visual of the stellar model template).

The width of the majority of the coronal lines is narrower than the widths of the broad permitted AGN emission lines (see Figure 16), as is expected from forbidden high-ionization collisionally-excited emission because it originates from a larger distance from the ionization source. However, there is no strong evidence that the coronal emission lines in ZTF18aajupnt/AT2018dyk are observed with widths between the BL and NL emission, as expected in the scenario in which gas is outflowing from an intermediate coronal line region (CLR; e.g. Mullaney & Ward 2008). The [Fe X] line is unlikely to be broader than expected due to blending with the [O I] $\lambda6364$ line (e.g. Pelat et al. 1987), as it is in a 1:3 ratio with the [O I] $\lambda6300$ line which is observed to be weaker than [Fe X] in this source. In Sy 1s, [Fe X] tends to be relatively stronger than the other coronal lines (e.g. Pfeiffer et al. 2000). However, in Seyferts the CL emission is typically measured to be only a few percent of the strength of [O III] $\lambda5007$.

The fact that [Fe X] $\lambda6374$ is stronger than [O III] $\lambda5007$ places ZTF18aajupnt/AT2018dyk away from other Seyferts and instead among the <10 known extreme coronal line emitters (ECLEs) in this parameter space. We discuss further the ECLE scenario in Section 4.2. We note that the weakness of [O III] may be due to light travel time effects, and thus may strengthen with time.
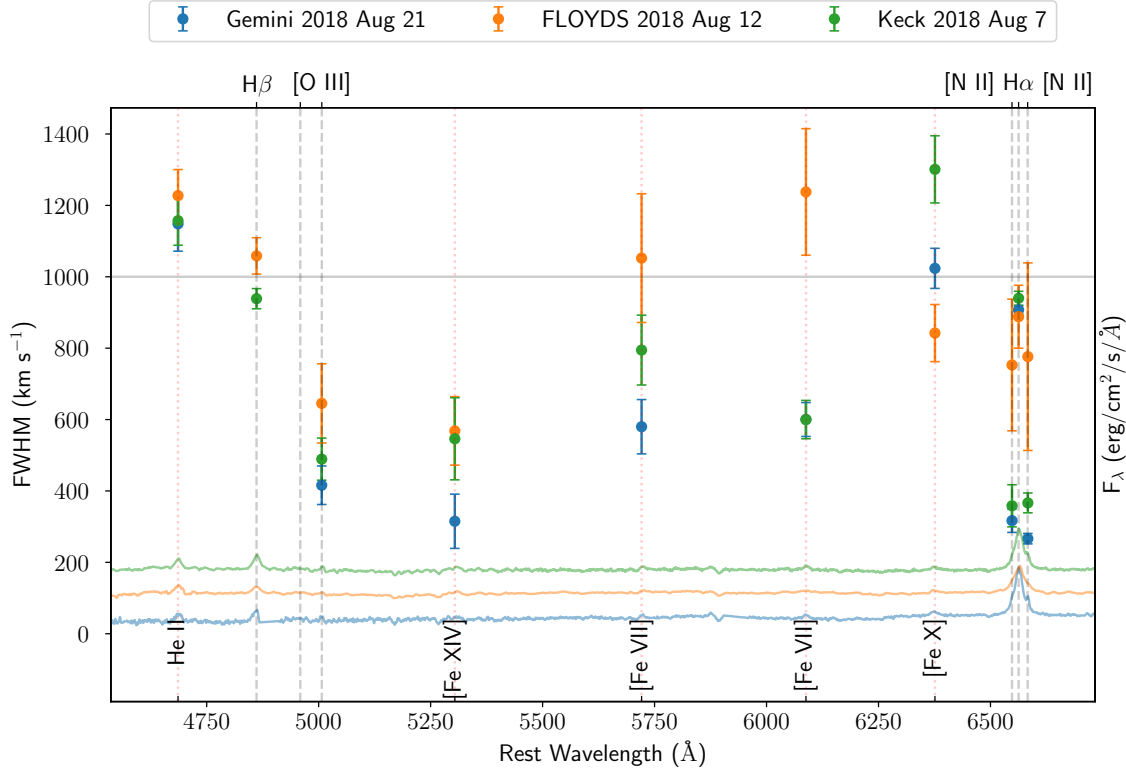
Figure 16. FWHM of Hα, Hβ, and the coronal lines for each high-resolution optical observation of ZTF18aajupnt/AT2018dyk in its "on" state. The stellar population of the host galaxy has been subtracted.

We note the significant spectral differences between ZTF18aajupnt/AT2018dyk and SN 2005ip post-peak (Smith et al. 2009). SN 2005ip has much more prominent coronal lines than even the example ECLEs, as well as a strong hydrogen emission series, much broader than the quasar iPTF16bco plotted alongside it.

Korista & Ferland (1998) presented a model by which coronal lines are the result of ISM interaction with bare Seyfert nuclei, i.e. AGN lacking any X-ray/UV evidence of intrinsic absorption by ionized gas along the line of sight to the AGN. This model is consistent with our finding of no intrinsic absorption in the X-ray spectra of ZTF18aajupnt/AT2018dyk.

3.6.2. *ZTF18aajupnt/AT2018dyk as a NLS1 in its "On" State*

At the other extreme of eigenvectors of AGN spectral properties are narrow-line Seyfert 1 galaxies (NLS1s), a subclass of AGN that are characterized by relatively narrow Balmer lines (FHWM < 2000 km s^{-1}), strong broad Fe II emission, [O III] $\lambda 5007$/H$\beta_{\rm tot}$ < 3, a prominent soft X-ray excess (e.g. Puchnarewicz et al. 1992), and dramatic variability, especially in the X-rays (e.g. Pogge 2000; Frederick et al. 2018). These spectral properties of NLS1s are attributed to lower-mass central black holes (5 < log($M_{\rm BH}[M_\odot]$) < 8; e.g. Mathur et al. 2001) that are thought to accrete at high Eddington ratios (Pounds et al. 1995; Wang et al. 1996; Grupe et al. 2010; Xu et al. 2012).

We measure $1000 \lesssim$ FWHM(Hβ) < 2000 km s^{-1} which is indicative of a narrow-line Seyfert 1 galaxy in the AGN interpretation (Goodrich 1989), as well as the fact that the Balmer lines are significantly better fits to Lorentzian line profiles than Gaussians (Nikołajuk et al. 2009). However, the FWHM limits between Sy 2s, NLS1s and Sy 1s is somewhat arbitrary (Véron-Cetty et al. 2001; Mullaney & Ward 2008), and may even be better set at 2200 km s^{-1} (Rakshit et al. 2017). The fact that some of the line measurements fall short of this cutoff could speak to the intermediate nature of this transitioning object in the changing-look scenario. The virial mass measurement for ZTF18aajupnt/AT2018dyk is consistent with the NLS1 interpretation, as NLS1s display properties consistent with AGNs with lower masses (Grupe & Mathur 2004), though it is toward the high end of the NLS1 mass distribution (Xu et al. 2012). Also consistent with the NLS1 scenario is that [O III] $\lambda 5007$ / Hβ = 0.1 < 3 (Osterbrock & Pogge 1985). However, [O III] $\lambda 5007$ appears to be relatively quite weak when compared to that of of prototypical NLS1, Mrk 618, in Figure 6. It should also be noted that the coronal lines in ZTF18aajupnt/AT2018dyk appear to be symmetric and at the same systematic redshift as the Balmer series and low-ionization forbidden lines, whereas coronal lines in Seyferts can be significantly broadened, asymmetric, and blueshifted consistent with an outflowing wind launched between the BLR and NLR (Rodríguez-Ardila et al. (2006);

in NLS1s: Erkens et al. (1997); Mullaney & Ward (2008); Porquet et al. (1999)). This is less common, but not unheard of, for ECLEs (See Section 4.2).

It is evident from all follow-up spectra of ZTF18aajupnt/AT2018dyk in Figure 6 that it is also missing the prominent Fe II pseudo-continuum complex characteristic of NLS1s. Therefore we do not utilize an Fe II template in subsequent optical nor UV spectral fitting. The intense ionizing radiation and high temperatures inferred from the presence of the coronal line emission should make visible the multiply ionized Fe II were it present. The fact that Fe II lags behind Hβ in reverberation mapping studies of AGN (Barth et al. 2013) could mean that not enough time has passed for this component to be irradiated, consistent with the weak presence of [O III] (Figure 17). Runnoe et al. (2016) also found that, for some CLAGN, the Fe II complex was only present in the "on" state. In AGN there is a robust negative correlation between [O III] and Fe II (the so-called Eigenvector 1; Boroson & Green (1992)), which manifests typically as weak [O III] in NLS1s (e.g. Rakshit et al. 2017), possibly indicating we should expect Fe II to become stronger in ZTF18aajupnt/AT2018dyk after the light-travel delay time.

Narrow He II is frequently observed in AGN, however we measure strong He II broader than the Balmer emission lines (Figure 16), possibly revealing an inner nuclear region not typically probed by the Balmer emission lines alone. This has been seen in a number of Seyferts such as the Sy1 Mrk 509, but is far less common.

He II $\lambda1640$ and [C III] $\lambda1909$ observed in the UV spectrum are consistent with the presence of higher ionization coronal lines in the optical. All prominent emission features are similar in strength and width to those in the *HST* FOS spectrum of NLS1 Mrk 335 and Mrk 478, shown in Figure 9 for comparison, however, with a Mg II $\lambda2798$, which is only marginally detected in the first *HST*/STIS epoch, and then brightens significantly 4 months later. However, like [O III], the late-time brightening of Mg II is likely a result of light travel time delays if the Mg II and [O III] line emitting gas resides further out from the central black hole.

3.6.3. *The Accretion Rate of ZTF18aajupnt/AT2018dyk*

The Eddington ratio of ZTF18aajupnt/AT2018dyk ranged between 0.02 and 0.09 from 2018 June to September, assuming the average BH mass of log $M_{BH}[M_\odot]$=7.1 (estimates described in Section 3.2 from stellar velocity dispersion as well as from the standard virial method; Shen et al. (2011)). Note that we assume a constant for the bolometric correction, but the SED is likely changing throughout the evolution of this source given the dramatic variability in α_{OX} described below. This L/L_{Edd} is toward the low end of the NLS1 distribution, and on the high end for that of CLQs (Xu et al. 2012; MacLeod et al. 2019). The range of Eddington ratios for the remainder of the sample is 0.03–0.8. ZTF18aajupnt/AT2018dyk is probing a critical inflection point in α_{OX} and Eddington ratio space related to

accretion rate driven state changes analogous to that of X-ray binaries (Ruan et al. 2019).

3.6.4. *X-ray Light Curve and Spectra of ZTF18aajupnt/AT2018dyk*

We initially measure a soft X-ray luminosity of a few $\times10^{41}$ erg s^{-1} from the first *Swift* XRT observations of ZTF18aajupnt/AT2018dyk on 2018 July 30. Wang et al. (2011) require at least a few $\times10^{42}$ erg s^{-1} to power the CLR, a level which ZTF18aajupnt/AT2018dyk did not reach until $\sim$40 days later. The XRT light curve in the lower panel of Figure 10 shows that ZTF18aajupnt/AT2018dyk is a variable X-ray source (we note that high-amplitude X-ray variability is characteristic of NLS1s; e.g. Nikołajuk et al. 2009). The excess variance (or fractional amplitude of variability) defined by Nandra et al. (1997) as $\sigma_{rms}^2 = \frac{1}{N\bar{x}} \sum_{i=1}^{N} (x_i - \bar{x})^2 - \delta x^2$ of the 0.3-10 keV 130-day light curve[11] is 0.41, similar to that of the most variable NLS1s, but high for Sy 1s (Grupe et al. 2000). We measure a maximum luminosity of $L_X = (3.7 \pm 0.4) \times 10^{42}$ erg s^{-1}. This X-ray luminosity is difficult to obtain with even the brightest supernova explosions, which have been observed up to $\sim 10^{41}$ erg s^{-1} (Immler & Lewin 2003), and it is toward the lower end for both Seyferts and NLS1s (Hasinger 2008). The hardness ratio light curve in the lower panel of Figure 10 shows that the X-ray flare is primarily in the soft band i.e. 0.3−1.5 keV, while the 1.5−10 keV light curve tracks the variability but with a much smaller amplitude. In contrast, the optical and UV photometry displays a plateau during this time, reminiscent of that of iPTF16bco (Figure 1, 5), before declining over several months in a manner similar to ZTF18aasszwr.

The simultaneous optical-to-X-ray spectral slope ratio (α_{OX}) defined as

$$\alpha_{OX} = 0.3838 \log(L_{2\,keV}/L_{2500A})$$

by Eq. 4 of Tananbaum et al. (1979), and Eq. 11 of Grupe et al. (2010), over several epochs, measures roughly how an object's SED is changing with time, and is strongly correlated with Eddington ratio (Poole et al. 2008). However, Grupe et al. (2010) argue that this correlation only a reliable estimator for Eddington ratio for sources with $\Gamma \leq 1.6$, above which the relationship saturates. We derive α_{OX} from the multi-epoch concurrent observations between 2018 July 30 (61 days after discovery) and Dec 08 by *Swift* XRT and UVOT (taken with the UVW2 filter, which has a central wavelength of 1928Å and FWHM 657Å; Poole et al. (2008)).

ZTF18aajupnt/AT2018dyk shows dramatic variability in the X-rays (rising by an order of magnitude in 5 months with L_X that varied between (0.4– 3.1) $\times10^{42}$ erg s^{-1}; see Figure 10). However, the range of α_{OX} for

---

[11] The detections used to compute the excess variance were in units of counts.
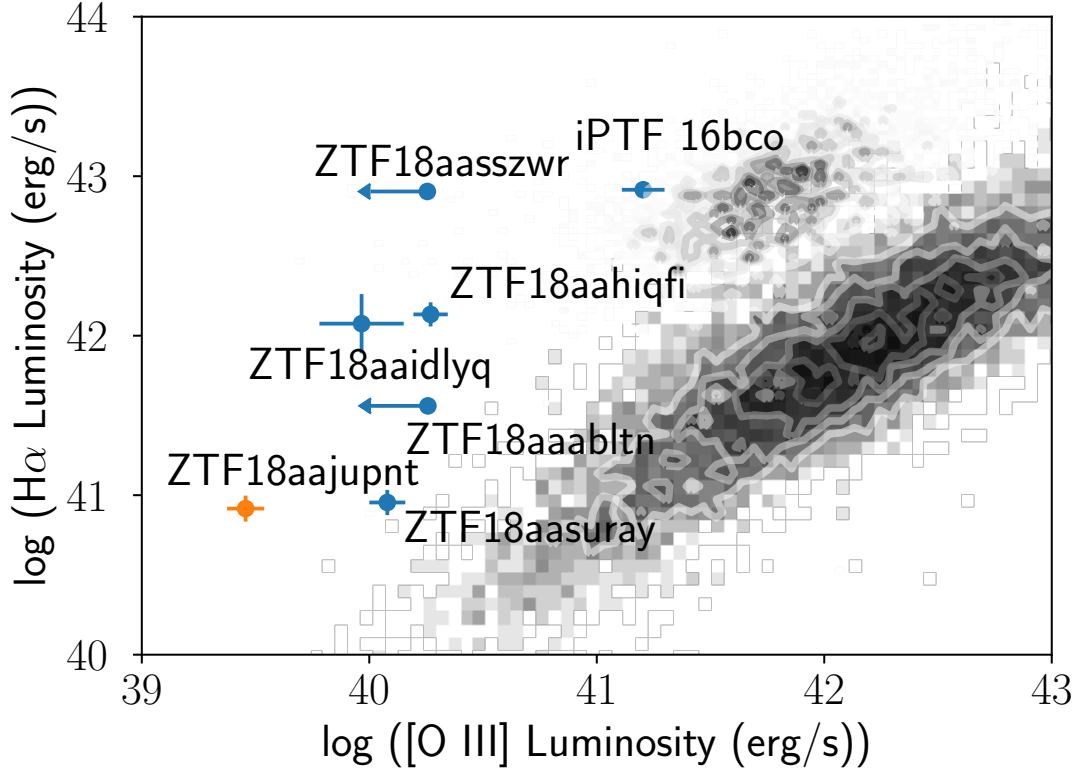
Figure 17. Hα and [O III] λ5007 line luminosities measured for this sample of CL LINERs, in the high state. The upper and lower contours representing log $L_{H\alpha}$ vs. log $L_{[O III]}$ measurements of SDSS DR7 quasars and Sy 1 galaxies from Shen et al. (2011) and Mullaney et al. (2013) show that this sample is up to an order of magnitude underluminous in [O III], due to light-travel time delays of an extended narrow line region that has yet to respond to the continuum flux change. The lower limits of ZTF18aasszwr and ZTF18aaabltn are due to the [O III] λ5007 emission line not being resolved in the low-resolution ($R \sim 100$) follow-up spectra. Adapted from Figure 6 in Gezari et al. (2017).

ZTF18aajupnt/AT2018dyk (-1.15−-0.67) is fairly consistent with that of typical LINER values ($-1.4 < \alpha_{OX} < -0.8$; Maoz (2007)) and systematically shallower than that of Type 1 Seyferts ($-2.0 < \alpha_{OX} < -1.2$ (Steffen et al. 2006; Elvis et al. 1994)) and most NLS1s ($-1.8 < \alpha_{OX} < -0.9$; Gallo (2006)).

The soft X-ray spectrum and coronal line emission in ZTF18aajupnt/AT2018dyk are shared characteristics with NLS1s. The soft X-ray component in excess above the extrapolation of hard X-ray power-law continuum is observed in a large fraction of Seyfert AGN (Singh et al. 1985), but is particularly strong in NLS1s. The full extent of the soft excess component remains unknown, and its origin is debated. It has been ruled out as the tail of the UV thermal emission from the accretion disk (Gierliński & Done 2004; Porquet et al. 2004; Piconcelli et al. 2005; Miniutti et al. 2009) but Comptonization of those seed photons is now one of the favored scenarios (e.g. Done et al. 2012), as is blurred ionized disk reflection García et al. (2019).

Due to their high ionization potentials ($\chi > 100$ eV), coronal lines can probe the soft X-ray excess indirectly, as well as the SED in the vicinity of 200 eV, which is difficult to observe otherwise because of both Galactic and intrinsic photoelectric absorption, but important due to their significant contribution to L_{bol}. Erkens et al. (1997) found that coronal lines were more likely to be present in Seyferts with steeper X-ray spectra. Gelbord et al. (2009) found in a sample of Seyfert galaxies a correlation between soft X-rays and [Fe VII], [Fe X], and [Fe XI] lines, proposed by Murayama & Taniguchi (1998a,b) to originate from the innermost wall of the dusty torus (see also Rodríguez-Ardila et al. (2002)).

NLS1s also display strong coronal line emission (e.g. Stephens 1989). Optical coronal lines include the forbidden transitions of iron, [Fe XIV] λ5304, [Fe VII] λ6088, [Fe X] λ6376 and [Fe XI] λ7894, as well as [Ar XIV] λ4414 and [S XII] λ7612. The coronal lines in NLS1s can be blueshifted with asymmetric velocity profiles and broad wings, consistent with an outflow (Erkens et al. 1997; Porquet et al. 1999; Nagao et al. 2000). Gelbord et al. (2009) found [Fe X]/[O III] to be the most extreme (by a factor of 2-3) in NLS1s with the narrowest broad lines (FWHM(Hα)$\sim$800 km s^{-1}) during a search for AGN with

strong coronal lines in SDSS, and interpreted these sources as having strong soft excesses.

4. DISCUSSION

While the number of CLAGN is steadily increasing, there has yet to be a large-scale systematic study of newly-discovered candidates that simultaneously tracks the appearance of continuum variability and the broad-line emission in real-time using high-cadence difference imaging photometry.

The best-studied target-of-interest in this sample was identified from ZTF based on its TDE-like rise time, and therefore we obtained several epochs of supporting data in real-time throughout its evolution. Its months-long plateau, UV/optical spectra, and high-energy properties were indicative of having changed look to a NLS1. Although they are typically highly X-ray variable, such dramatic optical variability of a NLS1 has only been seen in three other sources to-date, including CLAGN NGC 4051 (Guainazzi et al. 1998; Uttley et al. 1999), although it changed from an obscured Sy 2 and not a LINER. ZTF18aajupnt/AT2018dyk is therefore unique not only among this sample, but among CLAGN overall.

4.1. *A New Class of Changing Look LINERs*

We establish this particular class of CLAGN associated with extreme order-of-magnitude changes in continuum and emission line flux compared to less dramatic changing looks occurring in Seyferts (shown in Figure 14).

Although most CLAGN reported to-date are Seyferts, this may be due to sample selection bias, as the high numbers of LINERs may cause them to be seen as galaxy contaminants in such searches. Difference imaging offers a unique mechanism to discover variability in known LINERs.

4.2. *Is ZTF18aajupnt/AT2018dyk a TDE or AGN activity?*

We focus specifically on ZTF18aajupnt/AT2018dyk, which shows the appearance of broad Balmer and coronal lines within 16 years of being spectroscopically confirmed as a LINER, accompanied by an order-of-magnitude soft X-ray flare. Given a ROSAT All-Sky Survey flux upper limit of $F_{0.12.4\ keV} < 5 \times 10^{-13}$ ergs s^{-1} cm^{-2} at the location of the host from 1990 to 1991 (Voges et al. 1999), ZTF18aajupnt/AT2018dyk has therefore displayed a changing look in both the optical and X-ray usages of this term. The lower limit for this change in soft X-ray flux (0.1-2.4 keV) was by a factor of 7 at the time of the most recent observation.

Although highly photometrically variable on their own, flares due to non-AGN mechanisms are not unheard of in NLS1s. For example, CSS100217:102913+404220 displayed a high state ($M_V = -22.7$ at 45 days post-peak) accompanied by broad Hα and was interpreted either as a Type IIn SN (Drake et al. 2011) or TDE (Saxton et al. 2018) near the nucleus ($\sim$150 pc) of a NLS1. It eventually faded back to its original level after one year. PS16dtm (or iPTF16ezh/SN 2016ezh) was a $\sim 1.7 \times 10^4$ K, and

near-Eddington but X-ray-quiet nuclear transient with strong Fe II emission which plateaued over $\sim$100 days while maintaining a constant blackbody temperature. The event was interpreted as a TDE exciting the BLR in a NLS1 (Blanchard et al. 2017), although Oknyansky et al. (2018) claimed it may instead be a CLAGN transitioning into a Sy 1. No X-rays were observed during follow-up, dimming at least by an order of magnitude compared to archival observations, but were predicted to reappear after the obscuring debris had dissipated. SDSS J1233+0842 was discovered as a CLQ when it changed into a composite type galaxy or transition object (with [O III]/Hβ = -0.10 and [N II]/Hα = -0.17 from Figure 2.a. in MacLeod et al. (2019)). It shows variable Fe II emission (similar to PS16dtm), with the broad line emission disappearing between 2005 and 2016.

A nuclear transient in the nearby ULIRG F01004-2237 was classified as a TDE—despite an unusually long peak time of 1 year—partially based on the strength of its He II compared to Hβ (Tadhunter et al. 2017). This ratio was unprecedented for AGN activity, even for AGN in the high state of a changing look. We note that although it is broad, He II/H$\beta \sim 0.4$ for ZTF18aajupnt/AT2018dyk is far below that measured for F01004-2237. It was later argued that the nature of this transient may instead be due to changes in the accretion flow, similar to that of OGLE17aaj, which also showed a slow optical rise and long plateau and slow decline and UV and X-ray properties similar to that of ZTF18aajupnt/AT2018dyk, although it lacked spectral classification prior to discovery of the transient (Gromadzki et al. 2019). The transient AT2017bgt was classified as a dramatic SMBH UV/optical flare which irradiated the BLR and was interpreted as the result of increased accretion onto the SMBH (Trakhtenbrot et al. 2019). Unlike ZTF18aajupnt/AT2018dyk, it showed no decrease in flux over several months. The persistence of the UV emission distinguished it from SNe and TDEs, and the extremely intense nature of the UV continuum as well as presence of Bowen fluorescence He II, [N III] λ4640, and [O III] double-peaked features in the unobscured optical spectrum distinguished it from CLAGN. As in the "on" state of ZTF18aajupnt/AT2018dyk, the Balmer FWHM in all 3 sources are consistent with that of NLS1 galaxies.

ECLEs are most typically thought to be the echoes of TDEs via the accretion of tidal disruption streams by previously non-active SMBHs (Wang et al. 2012). However, less than 10 ECLEs have been reported in the literature, most notably SDSS J0952+2143 (Komossa et al. (2008, 2009); Palaversa et al. (2016); also technically a NLS1 using the unconventional cutoff in Rakshit et al. (2017), see Section 3.6.2 for details), and SDSS J0748+4712 (Wang et al. 2011). We confirm that ZTF18aajupnt/AT2018dyk is technically an "extreme" CLE by the definition put forth by Wang et al. (2012), because the strength of [Fe X] λ6376 is comparable to that of [O III] λ5007, as well as by the presence of [Fe XIV] in the optical spectrum (seen in Figures 6 and 21) following the independent definition of

Palaversa et al. (2016). We note, however, that it is the present weakness of [O III] that is driving this diagnostic, and the coronal lines overall do not appear nearly as strong when compared to the prototypical ECLEs, SDSS J0952+2143 and J0748+4712, in Figure 6. This strong, slowly variable transient nuclear coronal line emission necessitates soft X-ray flaring outbursts from an accretion disk, which may be formed as tidal debris settles, illuminating the outermost debris as well as intervening ISM (Komossa & Bade 1999). The coronal lines in these sources, some blueshifted, faded on timescales of 1-5 years, with strong [O III] appearing even later. Because strong coronal line emission is not a TDE diagnostic in isolation, some ECLE galaxies with persistent coronal lines may instead be Seyferts.

IC 3599 is an optical changing-look (displaying dramatic variability in not only Balmer lines but also [Fe VII] and [Fe XIV]) Sy 1.9 galaxy with strong soft X-ray repeating outbursts from its galactic nucleus which can be modeled by a disk instability with a rise time of ∼1 year whereby the inner disk is vacated and subsequently refills (Brandt et al. 1995; Grupe et al. 1995; Komossa & Bade 1999; Campana et al. 2015; Grupe et al. 2015). It is the only AGN which has shown fading of its coronal lines (though this variability is common among non-active ECLEs).

The *Swift*/XRT and *XMM* spectra of ZTF18aajupnt/AT2018dyk fit well to a steep power law (Γ ∼3±0.2) below 2 keV, not a disk blackbody as would be expected in the TDE scenario (see Figures 10 and 11). The large covering factor measured for ZTF18aajupnt/AT2018dyk by *Spitzer* is also more consistent with mid-infrared studies of CLAGN (Sheng et al. 2017), than the covering factor derived for TDEs with dust echoes (with $f_{\rm dust} = E_{\rm dust}/E_{\rm absorb}$ at the ∼1% level; van Velzen et al. 2016). This could imply appreciable accretion happening recently, because that is very likely required for a dusty torus with a large covering factor. In an accretion event unrelated to disk physics, a self-gravitating molecular cloud with low enough angular momentum could also be efficiently accreted on the correct timescales, activating radiation which subsequently illuminates the BLR (e.g. Hopkins et al. 2006). One way to obtain a larger covering factor would also be via chaotic cold accretion, by which interaction via inelastic collisions is made easier, boosting the funneling of molecular clumpy clouds toward the SMBH, and therefore enhancing the accretion rate (Gaspari & Sądowski 2017). The high blackbody temperature measured from UV spectroscopy implies the line of sight to the transient is not significantly dust obscured. Sheng et al. (2017) argue that mid IR light echoes of CLAGN (with $\Delta W1|W2 \gtrsim 0.4$ mag) was additional evidence to support the reprocessing scenario driven by changing accretion rate instead of variable obscuration. $W1 - W2$ for that sample varied between 0.1 and 1.2 mag, so $[3.6] - [4.5]$ $\mu m = 1.4$ mag for ZTF18aajupnt/AT2018dyk was consistent with the lowest end of that sample for mid IR color (it would not

have been selected based on its variability amplitude for the short duration of the *Spitzer* observations reported here).

LINERs may have inefficient accretion disks surrounding a low-luminosity AGN, occupying a unique physical parameter space compared to other CLAGN. Similar to the unification scheme derived for AGN (Antonucci 1993; Urry & Padovani 1995), broad- and narrow-line LINERs can be categorized into LINER1s and LINER2s (e.g. Ho et al. 1997a,b; González-Martín et al. 2015). Yan et al. (2019) reported the discovery of the "turning on" of a type 1 Seyfert occurring in LINER SDSS1115+0544 which flared for ∼1 year and subsequently plateaued, followed by a mid-IR dust echo delayed with respect to the optical by 180 days and a late-time UV flare, although no soft X-rays were detected then. Narrow coronal lines appeared in the spectrum along with Hα and Hβ consistent with broad line emission. As was done in Yan et al. (2019), we measured the soft X-ray-[Fe VII] ratio for ZTF18aajupnt/AT2018dyk to be log $L_{\rm 2\,keV}/L_{\rm [Fe\,VII]\lambda6088}$ =1.25 at maximum, still significantly below the average of 3.37 and pointing to an X-ray deficit compared to normal AGN (Gelbord et al. 2009), although we note that the soft X-rays changed by a factor of 10 and likely continued to rise beyond our last *Swift* observation. We also measure a minimum $L/L_{\rm Edd}$ equivalent to that of SDSS1115+0544. Yan et al. (2019) concluded an instability was required to "turn on" an AGN from a quiescent galaxy within hundreds of days. They argued that (despite a rate in tension with the AGN duty cycle) given the discovery of iPTF16bco and SDSS1115+0544 one year apart, such events should not be uncommon, a prediction this sample supports. There must be a connection between the LINER hosts and the state that is enabling these rapid transitions.

4.3. *The nature of the high-ionization forbidden "coronal" lines in ZTF18aajupnt/AT2018dyk*

Noda & Done (2018) posited that in the well-studied changing look AGN Mrk 1018, the coming and going of the soft X-ray excess (the main ionization source) drives the appearance and disappearance of the BLR and therefore the changing look phenomenon. We observe strong soft X-rays increasing in luminosity over time, which are required to form the coronal lines, although we note that the peak of the X-ray flaring appears to lag behind the UV/optical flaring.

The nuclear outburst in UV and X-ray required is similar to cataclysmic variable or black hole binary thermal-viscous disk instability flares, which have been discussed as a possible mechanism for powering optical changing-looks, although the observed time scales are much faster than predicted (e.g. Siemiginowska et al. 1996; Lawrence 2018; Stern et al. 2018; Ross et al. 2018).

Ross et al. (2018) attribute changing looks to a thermal (cooling) front propagating inward through the accretion disk or disk surface opacity changes, which have the correct timescales for observed transitions, unlike other proposed CLAGN mechanisms.

We posit that this quiet LINER suddenly goes into an active outbursting state, the rise in ionizing radiation at first

confined to the innermost BLR, turning on into a NLS1, then flash ionizing the ambient gas in the CLR, whereas the NLR (where [O III] and Fe II lines are formed) is at larger distances, and thus light-travel time effects delay their response. Mg II, though still broad, is formed further out on average (Goad et al. 1993; O'Brien et al. 1995; Cackett et al. 2015).

4.4. *The nature of the soft X-ray excess during the NLS1 state of ZTF18aajupnt/AT2018dyk*

The preceding interpretation does not explain the soft X-ray rise, which is clearly delayed at least ∼60 days with respect to the end of the UV/optical rise (shown in Figure 8), and may speak instead to a lag in an "outside-in" sense following the direction of an accretion flow, rather than photon propagation from a central "lamp post". This is in contrast to the clear inter-band time lags on the order of days in support of the reprocessing scenario measured by Shappee et al. (2014) in high cadence multiwavelength observations of CLAGN NGC 2617, which transitioned from a Sy 1.8 to a Sy 1 in 10 years. The ∼2 month lag observed in ZTF18aajupnt/AT2018dyk also suggests that this delay is not simply from light-travel time. X-ray inter-band time delays in NLS1s measured via Fourier based spectral timing, due to either X-ray reverberation or propagating fluctuations, are typically on the order of tens to hundreds of seconds (e.g. Uttley et al. 2014; Kara et al. 2016).

This delayed X-ray response may tell us something fundamental about the origin of the soft X-ray excess in AGN in general. The long delay of the soft X-ray flare relative to the expected light-travel time delays between the UV/optical emitting accretion disk and the compact, hot corona suggests that we are witnessing the real-time assembly of the corona plasma itself, possibly due to structural changes due to the dramatic change of state in the inner accretion disk (García et al. 2019).

If the Balmer emission is indeed from a BLR, we predict the Hα and Hβ lines should get broader as the UV luminosity decreases. Continued spectroscopic monitoring to look for evolution in line widths and strengths, particularly the narrow [O III] emission line and Mg II, and monitoring of the soft X-ray will be critical to map out the structure of this system and distinguish between the scenarios presented here.

5. CONCLUSIONS

We present the changing looks of six known LINERs caught turning on into type-1-like AGN found in Year 1 of the ZTF survey. It is the first systematic study of its kind performed in real time using difference imaging variability as the discovery mechanism for selecting nuclear transients in these previously quiescent galaxies.

1. We establish a class of changing look LINERs, distinct from Seyfert changing look AGN, with unique spectroscopic and photometric variability properties intrinsically due to the LINER environment.

2. This sample includes an multiwavelength study between 2018 June to 2019 March of the first case of a LINER changing look to a NLS1 — ZTF18aajupnt/AT2018dyk — which transitioned within 3 months based on its archival light curve.

3. We observed the delayed response of the NLR and broad Mg II with respect to the appearance of broad (yet < 2000 km s^{-1}) Balmer lines, and X-ray flaring delayed ∼60 days with respect to the optical/UV rise of this nuclear transient, indicative of an "outside-in" transition.

4. We interpret this particular object to be changing due to the accretion of material activating a pre-existing yet dormant accretion disk, which leads to the formation of a hot corona that then up-scatters the UV/optical seed photons to produce a soft X-ray excess.

This class of previously-weak AGN has the potential to be a laboratory with which to map out the structure of the accretion flow and surrounding environment. We plan to continue to monitor the behavior of these transients, and expect to build upon the sample at a rate of ∼4 year^{-1} for the next two years of the ZTF survey.

optical spectrograph has been funded by a generous grant from John and Ginger Giovale.

The W. M. Keck Observatory is operated as a scientific partnership among the California Institute of Technology, the University of California, and NASA; the Observatory was made possible by the generous financial support of the W. M. Keck Foundation.

Based on observations obtained at the Gemini Observatory, which is operated by the Association of Universities for Research in Astronomy (AURA) under a cooperative agreement with the NSF on behalf of the Gemini partnership: the National Science Foundation (United States), the National Research Council (Canada), CONICYT (Chile), the Australian Research Council (Australia), Ministerio da Ciencia e Tecnologia (Brazil) and Ministerio de Ciencia, Tecnologia e Innovacion Productiva (Argentina).

Based on observations made with the NASA/ESA Hubble Space Telescope, obtained from the data archive at the Space Telescope Science Institute. STScI is operated by the Association of Universities for Research in Astronomy, Inc. under NASA contract NAS 5-26555. These observations are associated with program 15331.

This work made use of data supplied by the UK Swift Science Data Centre at the University of Leicester.

This research has made use of the NASA/IPAC Extragalactic Database (NED) which is operated by the Jet Propulsion Laboratory, California Institute of Technology, under contract with the National Aeronautics and Space Administration.

Facilities: PO:1.2m, PO:1.5m, Hale, DCT, Keck:I (LRIS), Gemini:Gillett, HST (STIS), Swift, XMM

Software: HEAsoft (Arnaud 1996), SAS (Gabriel et al. 2004)

REFERENCES

Abolfathi, B., et al. 2018, ApJS, 235, 42

Agüeros, M. A., et al. 2005, AJ, 130, 1022

Antonucci, R. 1993, Annual Review of Astronomy and Astrophysics, 31, 473

Arcavi, I., et al. 2018, The Astronomer's Telegram, 11953

——. 2014, ApJ, 793, 38

Arnaud, K. A. 1996, in Astronomical Society of the Pacific Conference Series, Vol. 101, Astronomical Data Analysis Software and Systems V, ed. G. H. Jacoby & J. Barnes, 17

Baldi, R. D., Capetti, A., Robinson, A., Laor, A., & Behar, E. 2016, MNRAS, 458, L69

Barth, A. J., et al. 2013, ApJ, 769, 128

Bellm, E. C., et al. 2019a, PASP, 131, 018002

——. 2019b, pASP submitted

Bianchi, L., et al. 2005, ApJL, 619, L27

Blagorodnova, N., et al. 2017, ApJ, 844, 46

——. 2018a, arXiv e-prints, arXiv:1809.07446

——. 2018b, Publications of the Astronomical Society of the Pacific, 130, 035003

Blanchard, P. K., et al. 2017, ApJ, 843, 106

Boller, T., Brandt, W. N., & Fink, H. 1996, A&A, 305, 53

Bolzonella, M., Miralles, J.-M., & Pelló, R. 2000, A&A, 363, 476

Boroson, T. A., & Green, R. F. 1992, The Astrophysical Journal Supplement Series, 80, 109

Brandt, W. N., Pounds, K. A., & Fink, H. 1995, MNRAS, 273, L47

Bremer, M., Scharwächter, J., Eckart, A., Valencia-S., M., Zuther, J., Combes, F., Garcia- Burillo, S., & Fischer, S. 2013, A&A, 558, A34

Brown, J. S., et al. 2018, MNRAS, 473, 1130

Brown, P. J., et al. 2016, ApJ, 828, 3

Cackett, E. M., Gültekin, K., Bentz, M. C., Fausnaugh, M. M., Peterson, B. M., Troyer, J., & Vestergaard, M. 2015, ApJ, 810, 86

Campana, S., Mainetti, D., Colpi, M., Lodato, G., D'Avanzo, P., Evans, P. A., & Moretti, A. 2015, A&A, 581, A17

Cappellari, M. 2016, Annual Review of Astronomy and Astrophysics, 54, 597

Cappellari, M., & Emsellem, E. 2004, PASP, 116, 138

Cardelli, J. A., Clayton, G. C., & Mathis, J. S. 1989, ApJ, 345, 245

Cenko, S. B., et al. 2016, ApJL, 818, L32

——. 2006, Publications of the Astronomical Society of the Pacific, 118, 1396

Chang, Y.-Y., van der Wel, A., da Cunha, E., & Rix, H.-W. 2015, The Astrophysical Journal Supplement Series, 219, 8

Choi, Y., Gibson, R. R., Becker, A. C., Ivezić, Ž., Connolly, A. J., MacLeod, C. L., Ruan, J. J., & Anderson, S. F. 2014, ApJ, 782, 37

Cid Fernandes, R., Stasińska, G., Mateus, A., & Vale Asari, N. 2011, MNRAS, 413, 1687

Constantin, A., & Shields, J. C. 2003, Publications of the Astronomical Society of the Pacific, 115, 592

Corbett, E. A., Robinson, A., Axon, D. J., Hough, J. H., Jeffries, R. D., Thurston, M. R., & Young, S. 1996, MNRAS, 281, 737

Crenshaw, D. M., Kraemer, S. B., & Gabel, J. R. 2003, AJ, 126, 1690

da Cunha, E., Charlot, S., Dunne, L., Smith, D., & Rowlands, K. 2012, in IAU Symposium, Vol. 284, The Spectral Energy Distribution of Galaxies - SED 2011, ed. R. J. Tuffs & C. C. Popescu, 292–296

Davis, S. W., Woo, J.-H., & Blaes, O. M. 2007, ApJ, 668, 682

Done, C., Davis, S. W., Jin, C., Blaes, O., & Ward, M. 2012, MNRAS, 420, 1848

Drake, A. J., et al. 2011, ApJ, 735, 106

——. 2009, ApJ, 696, 870

Elitzur, M., & Ho, L. C. 2009, ApJ, 701, L91

Elitzur, M., Ho, L. C., & Trump, J. R. 2014, MNRAS, 438, 3340

Elvis, M., et al. 1994, ApJS, 95, 1

Eracleous, M., & Halpern, J. P. 2001, ApJ, 554, 240

Erkens, U., Appenzeller, I., & Wagner, S. 1997, A&A, 323, 707

Evans, P. A., et al. 2009, Monthly Notices of the Royal Astronomical Society, 397, 1177

Fazio, G. G., et al. 2004, The Astrophysical Journal Supplement Series, 154, 10

Filippenko, A. V. 1996, in Astronomical Society of the Pacific Conference Series, Vol. 103, The Physics of Liners in View of Recent Observations, ed. M. Eracleous, A. Koratkar, C. Leitherer, & L. Ho, 17

Forster, K., & Halpern, J. P. 1996, ApJ, 468, 565

Frederick, S., Kara, E., Reynolds, C., Pinto, C., & Fabian, A. 2018, ApJ, 867, 67

Gabriel, C., et al. 2004, in Astronomical Data Analysis Software and Systems (ADASS) XIII, Vol. 314, 759

Gallo, L. C. 2006, MNRAS, 368, 479

García, J. A., et al. 2019, ApJ, 871, 88

Gaspari, M., & Sądowski, A. 2017, ApJ, 837, 149

Gehrels, N., et al. 2004, ApJ, 611, 1005

Gelbord, J. M., Mullaney, J. R., & Ward, M. J. 2009, MNRAS, 397, 172

Gezari, S., et al. 2012, Nature, 485, 217

Gezari, S., et al. 2017, The Astrophysical Journal, 835

Gierliński, M., & Done, C. 2004, MNRAS, 349, L7

Goad, M. R., O'Brien, P. T., & Gondhalekar, P. M. 1993, MNRAS, 263, 149

González-Martín, O., et al. 2015, A&A, 578, A74

Goodrich, R. W. 1989, The Astrophysical Journal, 342, 224

Graham, M. J., et al. 2019, arXiv e-prints, arXiv:1902.01945

Gromadzki, M., et al. 2019, A&A, 622, L2

Grupe, D., Beuermann, K., Mannheim, K., Bade, N., Thomas, H.-C., de Martino, D., & Schwope, A. 1995, A&A, 299, L5

Grupe, D., Komossa, S., Leighly, K. M., & Page, K. L. 2010, ApJS, 187, 64

Grupe, D., Komossa, S., & Saxton, R. 2015, ApJL, 803, L28

Grupe, D., Leighly, K. M., Thomas, H.-C., & Laurent-Muehleisen, S. A. 2000, A&A, 356, 11

Grupe, D., & Mathur, S. 2004, ApJL, 606, L41

Guainazzi, M., et al. 1998, MNRAS, 301, L1

Häring, N., & Rix, H.-W. 2004, ApJL, 604, L89

Hasinger, G. 2008, A&A, 490, 905

Heckman, T. M. 1980, A&A, 500, 187

Hernández-Toledo, H. M., Vázquez-Mata, J. A., Martínez-Vázquez, L. A., Choi, Y.-Y., & Park, C. 2010, AJ, 139, 2525

Ho, L. C. 2009, The Astrophysical Journal, 699, 626

Ho, L. C., Filippenko, A. V., & Sargent, W. L. W. 1993, in American Astronomical Society Meeting Abstracts, Vol. 182, American Astronomical Society Meeting Abstracts #182, 17.05

Ho, L. C., Filippenko, A. V., & Sargent, W. L. W. 1997a, The Astrophysical Journal Supplement Series, 112, 315

Ho, L. C., Filippenko, A. V., Sargent, W. L. W., & Peng, C. Y. 1997b, The Astrophysical Journal Supplement Series, 112, 391

Holoien, T. W. S., Brown, J. S., Auchettl, K., Kochanek, C. S., Prieto, J. L., Shappee, B. J., & Van Saders, J. 2018, MNRAS, 480, 5689

Holoien, T. W. S., et al. 2016a, MNRAS, 463, 3813

——. 2016b, MNRAS, 455, 2918

Hopkins, P. F., Somerville, R. S., Hernquist, L., Cox, T. J., Robertson, B., & Li, Y. 2006, ApJ, 652, 864

Hung, T., et al. 2017, ApJ, 842, 29

——. 2018, The Astrophysical Journal Supplement Series, 238, 15

——. 2019, in preparation

Immler, S., & Lewin, W. H. 2003, in Supernovae and Gamma-Ray Bursters (Springer), 91–111

Kalberla, P. M., Burton, W., Hartmann, D., Arnal, E., Bajaja, E., Morras, R., & Pöppel, W. 2005, Astronomy & Astrophysics, 440, 775

Kara, E., Alston, W. N., Fabian, A. C., Cackett, E. M., Uttley, P., Reynolds, C. S., & Zoghbi, A. 2016, Mon. Not. R. Astron. Soc., 462, 511

Kasliwal, M. M., et al. 2019, PASP, 131, 038003

Kaspi, S., Smith, P. S., Netzer, H., Maoz, D., Jannuzi, B. T., & Giveon, U. 2000, ApJ, 533, 631

Kauffmann, G., et al. 2003, MNRAS, 346, 1055

Kewley, L. J., Heisler, C. A., Dopita, M. A., & Lumsden, S. 2001, The Astrophysical Journal Supplement Series, 132, 37

Komossa, S. 2002, Reviews in Modern Astronomy, 15, 27

Komossa, S., & Bade, N. 1999, A&A, 343, 775

Komossa, S., et al. 2009, ApJ, 701, 105

——. 2008, ApJ, 678, L13

Korista, K., & Ferland, G. 1998, ApJ, 495, 672

Kuminski, E., & Shamir, L. 2016, The Astrophysical Journal Supplement Series, 223, 20

Law, N. M., et al. 2009, Publications of the Astronomical Society of the Pacific, 121, 1395

Lawrence, A. 2018, Nature Astronomy, 2, 102

MacLeod, C. L., et al. 2019, ApJ, 874, 8

MacLeod, C. L., et al. 2016, Monthly Notices of the Royal Astronomical Society, 457, 389

Mahabal, A., et al. 2019, Publications of the Astronomical Society of the Pacific, 131, 038002

Maoz, D. 2007, MNRAS, 377, 1696

Marconi, A., Axon, D. J., Maiolino, R., Nagao, T., Pastorini, G., Pietrini, P., Robinson, A., & Torricelli, G. 2008, ApJ, 678, 693

Martin, D. C., et al. 2005, ApJ, 619, L1

Marziani, P., & Sulentic, J. W. 2012, New Astronomy Reviews, 56, 49

Masci, F. J., et al. 2017, Publications of the Astronomical Society of the Pacific, 129, 014002

——. 2019, PASP, 131, 018003

Mathur, S., et al. 2018, ApJ, 866, 123

Mathur, S., Kuraszkiewicz, J., & Czerny, B. 2001, NewA, 6, 321

McLure, R. J., & Dunlop, J. S. 2002, MNRAS, 331, 795

Mendel, J. T., Simard, L., Palmer, M., Ellison, S. L., & Patton, D. R. 2014, ApJS, 210, 3

Miller, J. M., et al. 2015, Nature, 526, 542

Miniutti, G., Ponti, G., Greene, J. E., Ho, L. C., Fabian, A. C., & Iwasawa, K. 2009, MNRAS, 394, 443

Molthagen, K., Bade, N., & Wendker, H. J. 1998, A&A, 331, 925

Mullaney, J. R., Alexander, D. M., Fine, S., Goulding, A. D., Harrison, C. M., & Hickox, R. C. 2013, MNRAS, 433, 622

Mullaney, J. R., & Ward, M. J. 2008, MNRAS, 385, 53

Murayama, T., & Taniguchi, Y. 1998a, ApJ, 503, L115

——. 1998b, ApJ, 497, L9

Nagao, T., Taniguchi, Y., & Murayama, T. 2000, AJ, 119, 2605

Nandra, K., George, I. M., Mushotzky, R. F., Turner, T. J., & Yaqoob, T. 1997, ApJ, 476, 70

Netzer, H., Mainieri, V., Rosati, P., & Trakhtenbrot, B. 2006, A&A, 453, 525

Nikołajuk, M., Czerny, B., & Gurynowicz, P. 2009, MNRAS, 394, 2141

Noda, H., & Done, C. 2018, MNRAS, 480, 3898

Nussbaumer, H., & Storey, P. J. 1979, A&A, 74, 244

O'Brien, P. T., Goad, M. R., & Gondhalekar, P. M. 1995, MNRAS, 275, 1125

Ofek, E. O., & Frail, D. A. 2011, ApJ, 737, 45

Oknyansky, V. L., et al. 2016, MNRAS, 000, 1

Oknyansky, V. L., Malanchev, K. L., & Gaskell, C. M. 2018, arXiv e-prints, arXiv:1810.08844

Osterbrock, D. E., & Pogge, R. W. 1985, The Astrophysical Journal, 297, 166

Palaversa, L., Gezari, S., Sesar, B., Stuart, J. S., Wozniak, P., Holl, B., & Ivezić, Ž. 2016, ApJ, 819, 151

Patterson, M. T., et al. 2019, PASP, 131, 018001

Pelat, D., Alloin, D., & Bica, E. 1987, A&A, 182, 9

Pfeiffer, M., Appenzeller, I., & Wagner, S. 2000, NewAR, 44, 547

Piconcelli, E., Jimenez-Bailón, E., Guainazzi, M., Schartel, N., Rodríguez-Pascual, P. M., & Santos-Lleó, M. 2005, A&A, 432, 15

Pogge, R. W. 2000, NewAR, 44, 381

Poole, T. S., et al. 2008, MNRAS, 383, 627

Porquet, D., Dumont, A.-M., Collin, S., & Mouchet, M. 1999, A&A, 341, 58

Porquet, D., Reeves, J. N., O'Brien, P., & Brinkmann, W. 2004, A&A, 422, 85

Pounds, K. A., Done, C., & Osborne, J. P. 1995, MNRAS, 277, L5

Puchnarewicz, E. M., et al. 1992, MNRAS, 256, 589

Rakshit, S., Stalin, C. S., Chand, H., & Zhang, X.-G. 2017, The Astrophysical Journal Supplement Series, 229, 39

Rau, A., et al. 2009, Publications of the Astronomical Society of the Pacific, 121, 1334

Rigault, M., et al. 2019, arXiv e-prints, arXiv:1902.08526

Rodríguez-Ardila, A., Prieto, M. A., Viegas, S., & Gruenwald, R. 2006, ApJ, 653, 1098

Rodríguez-Ardila, A., Viegas, S. M., Pastoriza, M. G., & Prato, L. 2002, ApJ, 579, 214

Roming, P. W. A., et al. 2005, SSRv, 120, 95

Ross, N. P., et al. 2018, MNRAS, 480, 4468

Ruan, J. J., et al. 2016, The Astrophysical Journal, 826

Ruan, J. J., Anderson, S. F., Eracleous, M., Green, P. J., Haggard, D., MacLeod, C. L., Runnoe, J. C., & Sobolewska, M. 2019, arXiv e-prints, arXiv:1903.02553

Rumbaugh, N., et al. 2018, ApJ, 854, 160

Runnoe, J. C., et al. 2016, MNRAS, 455, 1691

Sarzi, M., et al. 2017, GANDALF: Gas AND Absorption Line Fitting

Saxton, C. J., Perets, H. B., & Baskin, A. 2018, MNRAS, 474, 3307

Schawinski, K., Thomas, D., Sarzi, M., Maraston, C., Kaviraj, S., Joo, S.-J., Yi, S. K., & Silk, J. 2007, MNRAS, 382, 1415

Schlafly, E. F., & Finkbeiner, D. P. 2011, ApJ, 737, 103

Schlegel, D. J., Finkbeiner, D. P., & Davis, M. 1998, ApJ, 500, 525

Schneider, D. P., et al. 2010, AJ, 139, 2360

Shappee, B. J., et al. 2014, The Astrophysical Journal, 788

Shen, Y., & Ho, L. C. 2014, Nature, 513, 210

Shen, Y., et al. 2011, ApJS, 194, 45

Sheng, Z., Wang, T., Jiang, N., Yang, C., Yan, L., Dou, L., & Peng, B. 2017

Siemiginowska, A., Czerny, B., & Kostyunin, V. 1996, ApJ, 458, 491

Singh, K. P., Garmire, G. P., & Nousek, J. 1985, ApJ, 297, 633

Singh, R., et al. 2013, A&A, 558, A43

Smith, N., et al. 2009, ApJ, 695, 1334

Steffen, A. T., Strateva, I., Brandt, W. N., Alexander, D. M., Koekemoer, A. M., Lehmer, B. D., Schneider, D. P., & Vignali, C. 2006, AJ, 131, 2826

Stephens, S. A. 1989, AJ, 97, 10

Stern, D., et al. 2012, ApJ, 753, 30

——. 2018, ApJ, 864, 27

Stern, J., & Laor, A. 2012, MNRAS, 423, 600

Storchi-Bergmann, T., Baldwin, J. A., & Wilson, A. S. 1993, ApJL, 410, L11

Strüder, L., et al. 2001, Astronomy & Astrophysics, 365, L18

Tadhunter, C., Spence, R., Rose, M., Mullaney, J., & Crowther, P. 2017, Nature Astronomy, 1, 0061

Tananbaum, H., et al. 1979, ApJL, 234, L9

Thomas, D., et al. 2013, MNRAS, 431, 1383

Tonry, J. L., et al. 2018, Publications of the Astronomical Society of the Pacific, 130, 064505

Trakhtenbrot, B., et al. 2019, Nature Astronomy, 187

Tremaine, S., et al. 2002, ApJ, 574, 740

Urry, C. M., & Padovani, P. 1995, Publications of the Astronomical Society of the Pacific, 107, 803

Uttley, P., Cackett, E. M., Fabian, A. C., Kara, E., & Wilkins, D. R. 2014, A&A Rv, 22, 72

Uttley, P., McHardy, I. M., Papadakis, I. E., Guainazzi, M., & Fruscione, A. 1999, MNRAS, 307, L6

van Velzen, S., et al. 2011, ApJ, 741, 73

——. 2019, ApJ, 872, 198

van Velzen, S., Mendez, A. J., Krolik, J. H., & Gorjian, V. 2016, ApJ, 829, 19

Véron-Cetty, M.-P., Véron, P., & Gonçalves, A. C. 2001, A&A, 372, 730

Voges, W., et al. 1999, A&A, 349, 389

Wang, T., Brinkmann, W., & Bergeron, J. 1996, A&A, 309, 81

Wang, T.-G., Zhou, H.-Y., Komossa, S., Wang, H.-Y., Yuan, W., & Yang, C. 2012, ApJ, 749, 115

Wang, T.-G., Zhou, H.-Y., Wang, L.-F., Lu, H.-L., & Xu, D. 2011, ApJ, 740, 85

Wright, E. L., et al. 2010, AJ, 140, 1868

Xu, D., Komossa, S., Zhou, H., Lu, H., Li, C., Grupe, D., Wang, J., & Yuan, W. 2012, AJ, 143, 83

Yan, L., et al. 2019, arXiv e-prints, arXiv:1902.04163

APPENDIX
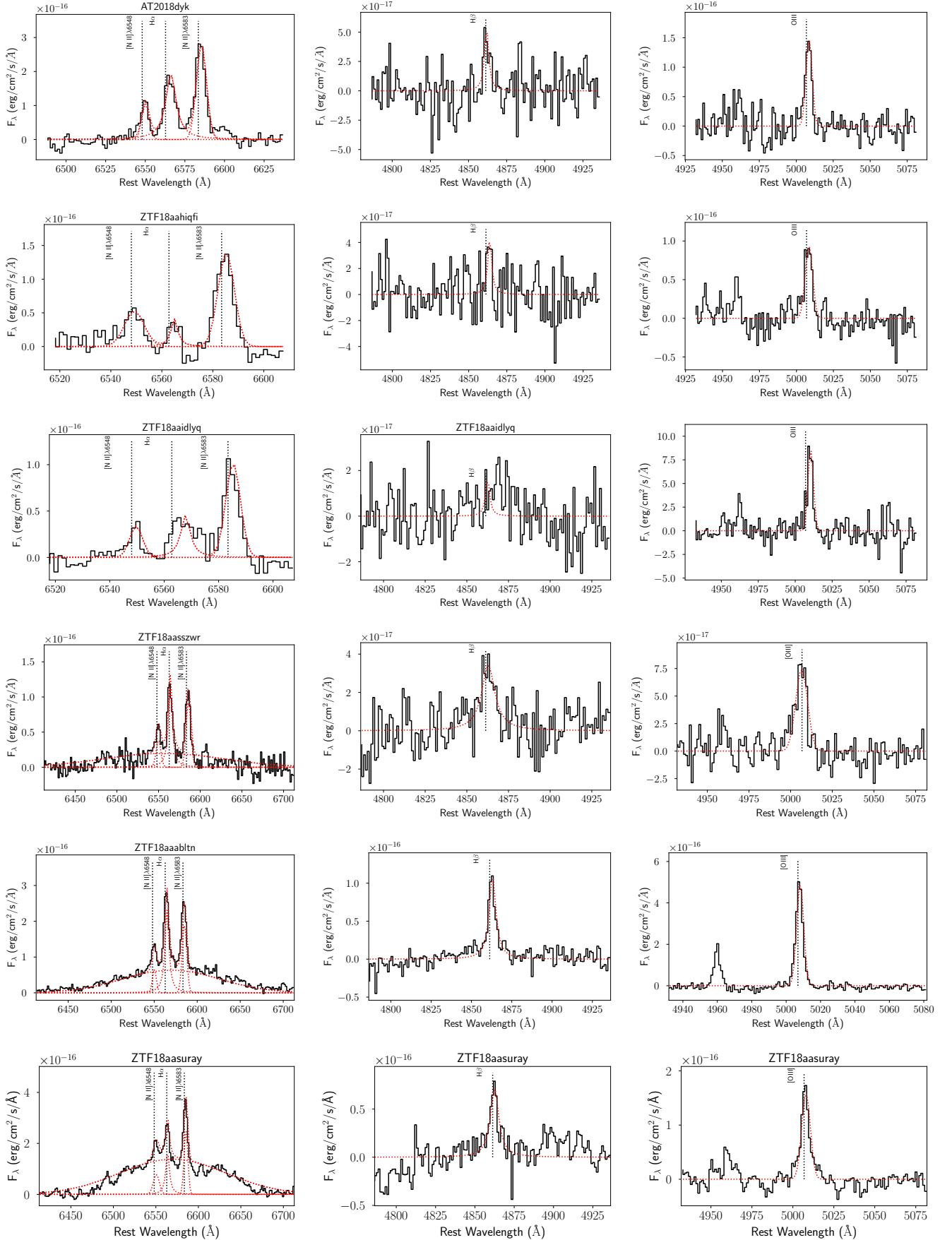
Figure 18. Stellar-continuum-subtracted Hα line complex, Hβ, and [O III] (first, second, and third columns, respectively) with best fits to Gaussians for the sample in their "off" state used in Figure 13. While fitting Hβ in ZTF18aaidlyq only, the FWHM in the model fit has been fixed to the FWHM of [N II] λ6585, due to Hβ being only marginally detected in that host. Note the differences in scale.
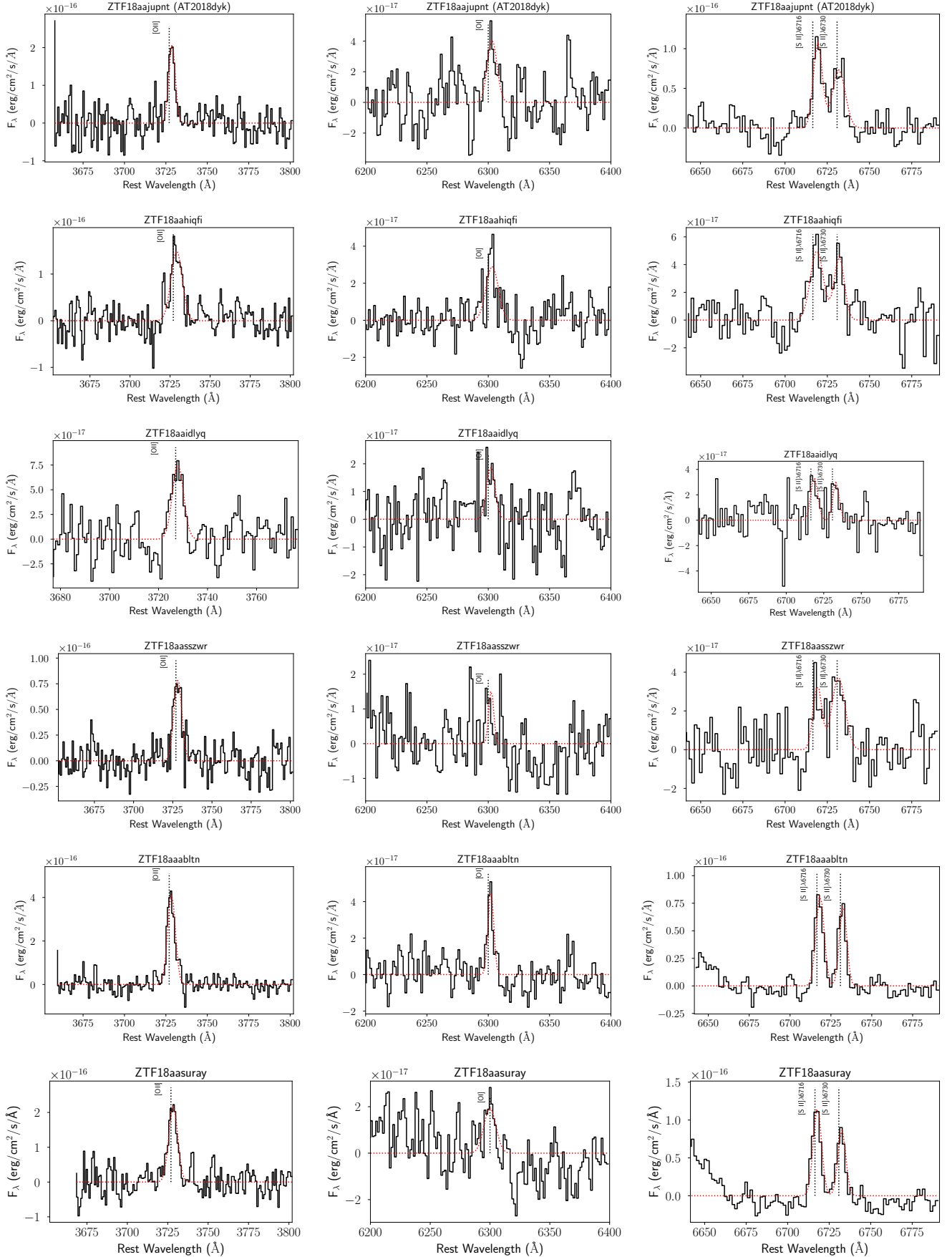
Figure 19. Stellar-continuum-subtracted [O II], [O I], and the [S II] doublet (first, second, and third columns, respectively) line profiles and best fits to Gaussians for the sample in their "off" state used in Figure 13. Note the differences in scale.
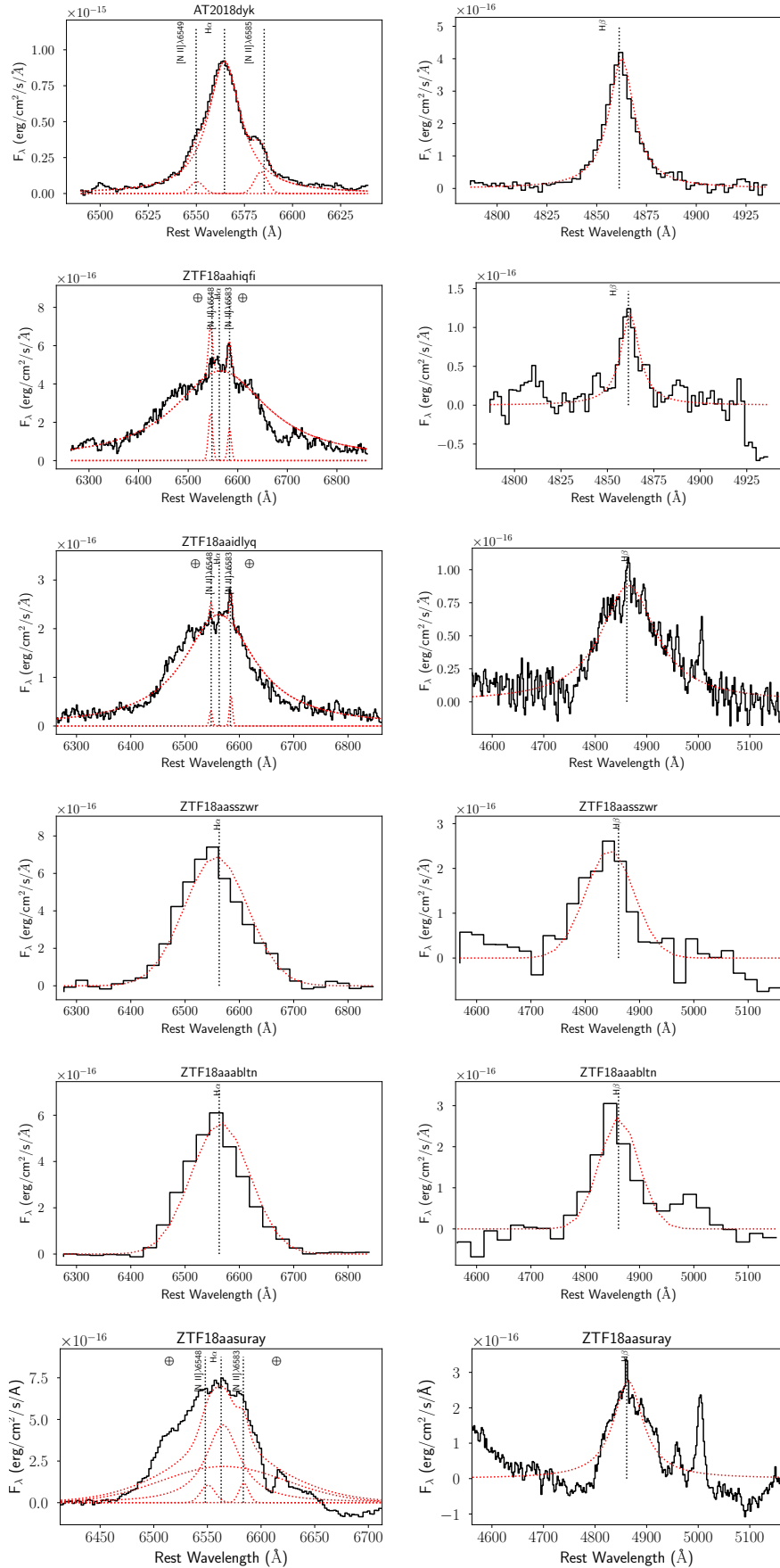
Figure 20. Balmer line profiles and best fits to Gaussians/Lorentzians for the sample in their "on" state. Note the difference in scales. See Section 2.5 for more details.
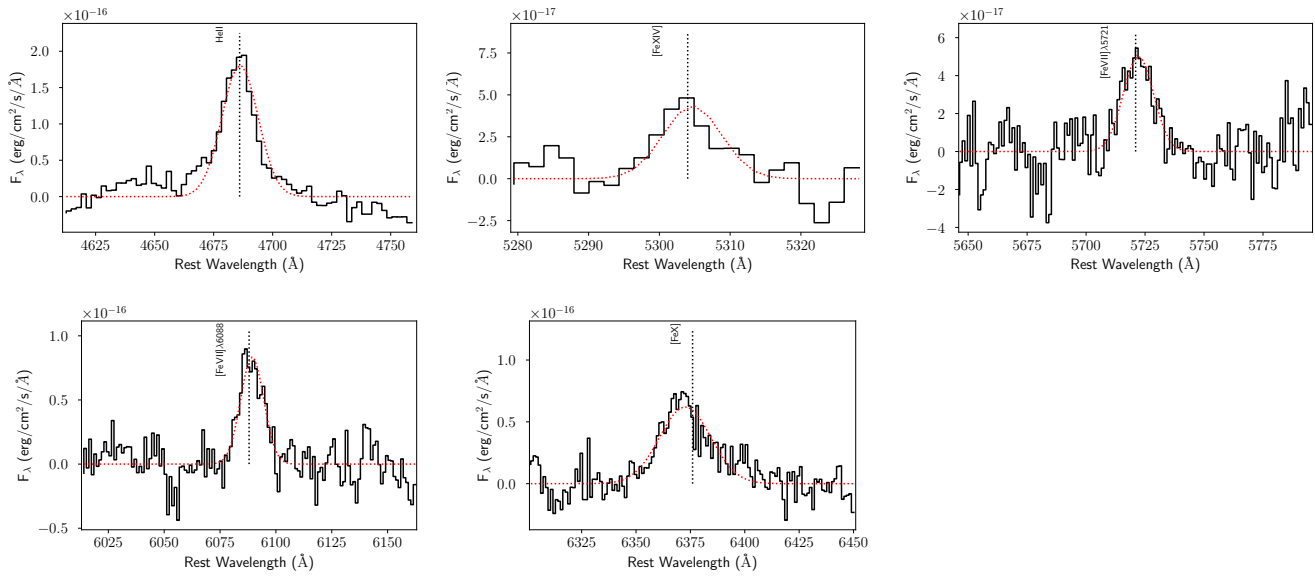
Figure 21. Coronal line profiles and best fits to Gaussians for the ZTF18aajupnt/AT2018dyk in its "on" state. The residual of the spectrum to the stellar continuum was fit. See Section 3.6.1 for more details.